

# The ultra-diffuse dwarf galaxies NGC 1052-DF2 and 1052-DF4 are in conflict with standard cosmology

Moritz Haslbauer<sup>1\*</sup>, Indranil Banik<sup>1</sup>, Pavel Kroupa<sup>1,2</sup> and Konstantin Grishunin<sup>3</sup>

<sup>1</sup>*Helmholtz-Institut für Strahlen- und Kernphysik, University of Bonn, Nussallee 14-16, D-53115 Bonn, Germany*

<sup>2</sup>*Faculty of Mathematics and Physics, Astronomical Institute, Charles University, V Holešovičkách 2, CZ-18000 Praha 8, Czech Republic*

<sup>3</sup>*Saint Petersburg State University, Universitetskii pr. 28, Saint Petersburg 198504, Russia*

Accepted 2019 August 13. Received 2019 July 3; in original form 2019 April 5

## ABSTRACT

Recently van Dokkum et al. (2018b) reported that the galaxy NGC 1052-DF2 (DF2) lacks dark matter if located at 20 Mpc from Earth. In contrast, DF2 is a dark-matter-dominated dwarf galaxy with a normal globular cluster population if it has a much shorter distance near 10 Mpc. However, DF2 then has a high peculiar velocity wrt. the cosmic microwave background of  $886 \text{ km s}^{-1}$ , which differs from that of the Local Group (LG) velocity vector by  $1298 \text{ km s}^{-1}$  with an angle of  $117^\circ$ . Taking into account the dynamical  $M/L$  ratio, the stellar mass, half-light radius, peculiar velocity, motion relative to the LG, and the luminosities of the globular clusters, we show that the probability of finding DF2-like galaxies in the lambda cold dark matter ( $\Lambda$ CDM) TNG100-1 simulation is at most  $1.0 \times 10^{-4}$  at 11.5 Mpc and is  $4.8 \times 10^{-7}$  at 20.0 Mpc. At 11.5 Mpc, the peculiar velocity is in significant tension with the TNG100-1, TNG300-1, and Millennium simulations, but occurs naturally in a Milgromian cosmology. At 20.0 Mpc, the unusual globular cluster population would challenge any cosmological model. Estimating that precise measurements of the internal velocity dispersion, stellar mass, and distance exist for 100 galaxies, DF2 is in  $2.6\sigma$  (11.5 Mpc) and  $4.1\sigma$  (20.0 Mpc) tension with standard cosmology. Adopting the former distance for DF2 and assuming that NGC 1052-DF4 is at 20.0 Mpc, the existence of both is in tension at  $\geq 4.8\sigma$  with the  $\Lambda$ CDM model. If both galaxies are at 20.0 Mpc the  $\Lambda$ CDM cosmology has to be rejected by  $\geq 5.8\sigma$ .

**Key words:** Galaxy: formation – Galaxy: fundamental parameters – globular clusters: general – galaxies: abundances – galaxies: individual: NGC 1052-DF2 – dark matter

## 1 INTRODUCTION

In the standard hierarchical bottom-up cosmological model, dwarf galaxies void of dark matter are formed in the overdensities of tidal tails and arms during interactions of massive galaxies. The high velocity dispersion of dark matter particles and the relatively shallow gravitational potential compared to their host galaxy prevent tidal dwarf galaxies (TDGs) to capture a significant amount of dark matter (Barnes & Hernquist 1992; Bournaud & Duc 2006; Wetzstein et al. 2007; Bournaud et al. 2008a,b; Fouquet et al. 2012; Yang et al. 2014; Ploekinger et al. 2018; Haslbauer et al. 2019).

The Dual Dwarf Theorem states that in any viable cosmological model, interactions between galaxies imply that

both primordial and TDGs must exist. In particular, the lambda cold dark matter ( $\Lambda$ CDM) cosmological model predicts both dark-matter-dominated dwarf galaxies and dark-matter-lacking TDGs with different observed stellar half-mass radii (Kroupa et al. 2010; Kroupa 2012; Dabringhausen & Kroupa 2013; Haslbauer et al. 2019). The former are primordial galaxies formed by the condensation of gas in dark matter halos. Dark-matter-dominated and dark-matter-poor dwarf galaxies (i.e. TDGs) are distinguishable in a radius–mass plane, because TDGs are formed naked without the help of dark matter and have to be therefore more compact in order to remain gravitationally bound (Kroupa 2012; Dabringhausen & Kroupa 2013; Haslbauer et al. 2019).

Ploekinger et al. (2018) demonstrated that TDGs can be found in the self-consistent cosmological EAGLE simulation and the study of TDG formation in the Illustris-1 sim-

\* E-mail: mhaslbauer@astro.uni-bonn.de (MH)

ulation by [Haslbauer et al. \(2019\)](#) contains a very detailed analysis of their properties as well as of resolution issues.

[van Dokkum et al. \(2018b\)](#) reported that the ultra-diffuse dwarf galaxy (UDG) NGC 1052-DF2 (hereafter DF2<sup>1</sup>) lacks dark matter based on velocity measurements of 10 globular clusters (GCs). They derive a velocity dispersion of  $\sigma_{\text{intr}} < 10.5 \text{ km s}^{-1}$  with 90% confidence corresponding to a total mass of  $M_{\text{total}} < 3.4 \times 10^8 M_{\odot}$  within a radius of 7.6 kpc, a stellar mass of  $M_* = 2 \times 10^8 M_{\odot}$  by assuming a mass-to-light ratio of  $M/L_V \approx 2 \Upsilon_{\odot}$ , and an effective radius along the major axis of  $R_e = 2.2 \text{ kpc}$  ([van Dokkum et al. 2018b](#)) corresponding to a 3D stellar half-light radius of<sup>2</sup>  $R_{1/2} = 2.7 \text{ kpc}$ .

Such an observation of a dark matter deficient galaxy would support that dark matter is indeed separable from dwarf galaxies and would therewith be consistent with the  $\Lambda$ CDM paradigm if it is a TDG. [Nusser \(2019\)](#) showed that tidal stripping of the outer dark matter halo of a primordial dwarf galaxy caused by the close galaxy NGC 1052 might also account for the low velocity dispersion of DF2. Such a process would be included in the hydrodynamical simulations.

Nevertheless, the intrinsic velocity dispersion of DF2 is rather uncertain. [Martin et al. \(2018\)](#) calculate a 90% upper limit of  $\sigma_{\text{intr}} < 17.3 \text{ km s}^{-1}$  implying  $M/L_V < 8.1 \Upsilon_{\odot}$ , which is comparable with the mass-to-light ratio of dwarf galaxies in the Local Group (LG) and allows a significant amount of dark matter ([Martin et al. 2018](#)). In a following paper [van Dokkum et al. \(2018a\)](#) revised the velocity of the globular cluster GC-98 and derived a new intrinsic velocity dispersion of  $\sigma_{\text{intr}} < 12.4 \text{ km s}^{-1}$  at 90% confidence concluding that ‘[it] is impossible to say whether the galaxy has no dark matter at all but it is clearly extremely dark matter deficient’ ([van Dokkum et al. 2018a](#)). A very low intrinsic velocity dispersion of around  $\sigma_{\text{intr}} = 7.8^{+5.2}_{-2.2} \text{ km s}^{-1}$  ([van Dokkum et al. 2018a](#)) of an isolated dwarf galaxy would be, according to [van Dokkum et al. \(2018b\)](#), in major conflict with modified gravity theories such as Milgromian dynamics (MOND, [Milgrom 1983](#)). However, DF2 is close to the massive elliptical galaxy NGC 1052 and taking into account its external field (which is an important prediction of MOND), DF2 becomes well consistent with MOND ([Famaey et al. 2018](#); [Kroupa et al. 2018](#); [Haghi et al. 2019](#); [Müller et al. 2019](#)). In fact, DF2 is extremely gas-depleted and could be therefore a satellite of NGC 1052, having lost its gas reservoir via ram-pressure stripping and tidal forces triggered by several close encounters ([Chowdhury 2019](#); [Sardone et al. 2019](#)).

Based on the surface brightness fluctuation (SBF) method, a distance for DF2 of  $D = 19.0 \pm 1.7 \text{ Mpc}$  from Earth has been derived ([van Dokkum et al. 2018d](#)). However, within the integrated galaxy-wide initial mass function (IGIMF) theory ([Kroupa & Weidner 2003](#); [Yan et al. 2017](#); [Jeřábková et al. 2018](#)), the IMF depends on the star formation rate (SFR). Therefore, dwarf galaxies that have a

low SFR will have a top-light IGIMF compared to massive galaxies ([Watts et al. 2018](#)). This would result in a lower number of giant stars, possibly making DF2 appear to be further away than it actually is ([Zonoozi et al. in prep](#)). Even without the IGIMF theory [Trujillo et al. \(2019\)](#) obtained a much smaller distance of  $D = 14.7 \pm 1.7 \text{ Mpc}$  by using the SBF method.

The apparent lack of dark matter and the unusually high luminosity of GC-like objects surrounding DF2 only hold if this dwarf galaxy is indeed located at a distance of approximately  $D = 20 \text{ Mpc}$  from Earth. A revised distance of about  $D = 10 \text{ Mpc}$  would make DF2 a usual dark-matter-dominated dwarf galaxy with  $M/L_V = 16.2 \Upsilon_{\odot}$  (assuming the velocity dispersion derived in [Martin et al. 2018](#)) and a GC population comparable to that of other galaxies ([Haghi et al. 2019](#); [Trujillo et al. 2019](#)). However, at such a small distance DF2 has a large radial peculiar velocity of about  $v_{\text{pec}} = 886 \text{ km s}^{-1}$  with respect to (wrt.) the cosmic microwave background (CMB) and a velocity of  $v_{\text{rel}} = 1298 \text{ km s}^{-1}$  relative to the motion of the LG. Such a high velocity is highly unlikely in the standard  $\Lambda$ CDM cosmological model which is based on Newtonian dynamics. A possible tension with the  $\Lambda$ CDM paradigm and a qualitative comparison to the predicted velocity field in MOND cosmological simulations conducted by [Candlish \(2016\)](#) are investigated inter alia in this work (see Sections 3.1 and 4.1.2). In the real Universe it is supposed that most of the peculiar velocity of the LG ( $v_{\text{pec,LG}} = 627 \pm 22 \text{ km s}^{-1}$  wrt. the CMB rest frame, [Kogut et al. 1993](#)) arises from a putative Great Attractor (GA) being about 62 Mpc away from us ([Lynden-Bell et al. 1988](#)). Within this distance from the Earth we should thus not expect large directional differences between galaxies that have large peculiar velocities, these being presumably generated by the GA.

The exact internal velocity dispersion and thus the dark matter content of DF2 remains controversial. Using the Multi Unit Spectroscopic Explorer (MUSE) at the VLT two ESO teams performed the first spectroscopic measurement of the stellar body of DF2 and discovered planetary nebulae (PNe) for the first time in an UDG ([Emsellem et al. 2019](#); [Fensch et al. 2019](#)). Using the Jeans model, [Emsellem et al. \(2019\)](#) obtain  $M/L_V$  ratios between  $3.5 - 3.9 (\pm 1.8) \Upsilon_{\odot}$ , which is close to the  $2\sigma$  upper limit of the results by [Martin et al. \(2018\)](#).

In contrast to that, [Danieli et al. \(2019\)](#) measured the stellar kinematics of DF2 with the Keck Cosmic Web Imager and derived, assuming  $D = 20 \text{ Mpc}$ ,  $M_* = (1.0 \pm 0.2) \times 10^8 M_{\odot}$ , a dynamical mass of  $M_{\text{dyn}} = (1.3 \pm 0.8) \times 10^8 M_{\odot}$  within the 3D half-light radius of  $R_{1/2} = 2.7 \text{ kpc}$ . In such a situation DF2 would indeed be an outlier compared to dwarf galaxies in the LG (see also fig. 5 in [Danieli et al. 2019](#)).

[Trujillo et al. \(2019\)](#) concluded that DF2 has a revised distance of  $13.0 \pm 0.4 \text{ Mpc}$  based on five redshift-independent distance indicators including the tip of the red giant branch (TRGB,  $D = 13.4 \pm 1.1 \text{ Mpc}$ ) and the SBF method ( $D = 14.7 \pm 1.7 \text{ Mpc}$ ), which were obtained with data from the Hubble space telescope (HST). They also estimated the distances using the luminosities and sizes of its GCs, and a comparison of the stellar luminosity function with that of the galaxy DDO44, which is similar to DF2. They obtain  $R_e = 1.4 \pm 0.1 \text{ kpc}$ ,  $M_* = 6 \times 10^7 M_{\odot}$ ,  $M_{\text{tot}} \gtrsim 10^9 M_{\odot}$ , and

<sup>1</sup> For the historical record of when this galaxy was discovered see [Trujillo et al. \(2019\)](#).

<sup>2</sup> The effective radius along the semimajor axis of DF2 can be converted to a 3D circularized half-mass radius by  $R_{1/2} \approx \frac{4}{3} R_e \sqrt{b/a}$ , where  $b/a$  is the axis ratio being 0.85 for DF2 ([Wolf et al. 2010](#); [van Dokkum et al. 2018b](#)).

$M_{\text{halo}}/M_* > 20$  such that DF2 would be consistent with dwarf galaxies of the LG (see fig. 29 in Trujillo et al. 2019).

van Dokkum et al. (2019) report the discovery of a second dark matter lacking galaxy, NGC 1052-DF4 (DF4), with an intrinsic velocity dispersion of  $\sigma_{\text{intr}} = 4.2^{+4.4}_{-2.2}$  km s<sup>-1</sup> located close to NGC 1052 and NGC 1042 in sky projection. Assuming a distance of 20 Mpc this galaxy has a mass within the outermost GC of  $M_{\text{TME}}(R < 7 \text{ kpc}) = 0.4^{+1.2}_{-0.3} \times 10^8 M_{\odot}$  estimated by the tracer mass estimator method,  $M_* = (1.5 \pm 0.4) \times 10^8 M_{\odot}$ ,  $b/a = 0.89$ ,  $R_e = 1.6$  kpc, and a GC population similar to that in DF2 (i.e. all seven identified GCs of DF4 have absolute magnitudes  $M_{V,606} \leq -8.6$  mag).

The unusual properties of DF2 (and of DF4) and its observed peculiar velocity constrain theoretical cosmology which must account for its existence. In this work we take into account the dynamical M/L ratio, structural property, mass, peculiar velocity, motion relative to the LG, and the GC population of these dwarfs. We concentrate mostly on DF2 because it has better observational constraints at present than DF4. By using simulations of the Illustris (Nelson et al. 2015), “The Next Generation” (TNG) Illustris (Nelson et al. 2019), and EAGLE (Schaye et al. 2015) projects, we assess the existence of a DF2-like galaxy in the  $\Lambda$ CDM framework over a wide range of distances.

The structure of the paper is as follows: In Section 2 we briefly introduce the Illustris, IllustrisTNG, and EAGLE simulations. The probabilities of detecting a DF2-like galaxy in these simulation runs and a study of its GC population are given in Section 3. In Section 4 we discuss our results and their implication for the  $\Lambda$ CDM paradigm including a comparison of the peculiar velocity field in IllustrisTNG and Millennium  $\Lambda$ CDM simulations and in MOND. This is followed by a conclusion in Section 5. Throughout this work we adopt for observed quantities a Hubble constant of  $H_0 = 70 \text{ km s}^{-1} \text{ Mpc}^{-1}$  at the present time.

## 2 METHODS

In this section we briefly introduce the Illustris-1, IllustrisTNG, and EAGLE cosmological simulations and describe the selection criteria and search-algorithm for simulated DF2- and DF4-like dwarf galaxies. In Section 4.1.2 we also employ the much larger (685 cMpc side) box of the Millennium simulation to quantify robustly the peculiar velocity field in a  $\Lambda$ CDM cosmology.

In the Illustris, IllustrisTNG, and EAGLE projects, comprehensive physical models are implemented allowing a detail study of galaxy formation and evolution in a self-consistent context across cosmic time. We stress that the Illustris and EAGLE simulations are completely independent from each other based on different codes and with different feedback recipes in galaxy evolution models (Genel et al. 2014; Vogelsberger et al. 2014a; Schaye et al. 2015). Dark matter halos are identified with the standard friends-of-friends (FOF) algorithm (Davis et al. 1985) and subhaloes within halos are detected with the Subfind algorithm (Springel et al. 2001; Dolag et al. 2009). Their physical properties are listed in the halo and subhalo catalogues, which can be downloaded from the Illustris and EAGLE webpages (Genel et al. 2014; Vogelsberger et al. 2014a; Schaye et al. 2015; Nelson et al. 2019). An overview about the physical

and numerical parameters of the mentioned simulation runs are given in Table 1.

### 2.1 Illustris and IllustrisTNG simulations

The Illustris (Nelson et al. 2015) and IllustrisTNG (Nelson et al. 2019) simulations are performed with the moving-mesh code AREPO (Springel 2010) and are based on a flat  $\Lambda$ CDM cosmology consistent with the Wilkinson Microwave Probe (WMAP)-9 (Hinshaw et al. 2013) and the Planck intermediate results (Planck Collaboration et al. 2016), respectively. We use the Illustris-1 and TNG100-1 simulations, of which each evolves  $2 \times 1820^3$  particles or gas cells in a cube with a co-moving length of  $75 h^{-1}$  cMpc (Vogelsberger et al. 2014b; Nelson et al. 2015, 2019). In order to include also large-scale waves to get an accurate estimate on the peculiar velocity of subhaloes (see Section 4.1.2), we also employ the TNG300-1 simulation which has a co-moving box length of  $205 h^{-1}$  cMpc. Both projects use different galaxy/physics models and compared to Illustris, IllustrisTNG includes magnetic fields (magnetohydrodynamical simulations) and has major modifications in the growth and feedback of supermassive black holes, galactic winds, and stellar evolution and gas chemical enrichment (Marinacci et al. 2018; Naiman et al. 2018; Nelson et al. 2018; Pillepich et al. 2018b; Springel et al. 2018). A detailed description about the IllustrisTNG galaxy models can be found in Pillepich et al. (2018a).

### 2.2 EAGLE simulations

The EAGLE simulations (Schaye et al. 2015) are performed with a modification of the GADGET-3 (Springel 2005) smoothed particle hydrodynamics code and with an implemented flat  $\Lambda$ CDM cosmology consistent with the initial Planck satellite data release (Planck Collaboration et al. 2014). Three different EAGLE simulation runs are used here as detailed in Table 1. EAGLE-1 is the largest simulation with a co-moving length of 100 cMpc per side and evolves  $2 \times 1504^3$  particles across cosmic time (Schaye et al. 2015). EAGLE-2 and EAGLE-3 are high-resolution runs performed in a simulation box with a co-moving length of 25 cMpc and  $2 \times 752^3$  particles. The main difference between those two simulations is that in EAGLE-3 the stellar and active galactic nucleus feedback parameters are re-calibrated such that the galaxy stellar mass function fits the observations, i.e. EAGLE-2 predicts two times more galaxies  $M_* > 10^9 M_{\odot}$  compared to observations of the local Universe (Schaye et al. 2015; McAlpine et al. 2016; Ploekinger et al. 2018).

### 2.3 Selection criteria and search-algorithm for DF2- and DF4-like dwarf galaxies

The here developed search-algorithm is sensitive to DF2- and DF4-like subhaloes based on their internal structures, masses, peculiar velocities, and motions relative to LG-like subhaloes scaled for different distances at redshift  $z = 0$ .

Low-mass subhaloes can be substructures embedded in the galactic disc of a massive host galaxy (Graus et al. 2018; Ploekinger et al. 2018; Haslbauer et al. 2019). Therefore, the algorithm removes in the first step subhaloes which are

**Table 1.** Physical and numerical parameters of the Illustris-1, TNG100-1, and TNG300-1 simulations and different runs of the EAGLE project.  $L$  is the co-moving length of the simulation box,  $N$  is the total number of particles or cells,  $H_0$  is the Hubble constant,  $\Omega_m$  is the total matter density,  $\Omega_b$  is the baryonic matter density,  $\Omega_\Lambda$  is the dark energy density at present time, and  $m_b$  and  $m_{dm}$  are the initial baryonic and dark matter particle masses, respectively. The gas cell resolution in Illustris-1 is 48 pc and in TNG100-1 (TNG300-1) the smallest gas cells have a radius of 14 pc (47 pc).

Simulation	$L$ [cMpc]	$N$	$H_0$ [km s $^{-1}$ Mpc $^{-1}$ ]	$\Omega_m$	$\Omega_b$	$\Omega_\Lambda$	$m_b$ [ $M_\odot$ ]	$m_{dm}$ [ $M_\odot$ ]
Illustris-1	106.5	$2 \times 1820^3$	70.4	0.2726	0.0456	0.7274	$1.3 \times 10^6$	$6.3 \times 10^6$
Illustris TNG100-1	110.7	$2 \times 1820^3$	67.74	0.3089	0.0486	0.6911	$1.4 \times 10^6$	$7.5 \times 10^6$
Illustris TNG300-1	302.6	$2 \times 2500^3$	67.74	0.3089	0.0486	0.6911	$1.1 \times 10^7$	$5.9 \times 10^7$
EAGLE-1 Ref-L0100N1504	100	$2 \times 1504^3$	67.77	0.307	0.04825	0.693	$1.81 \times 10^6$	$9.70 \times 10^6$
EAGLE-2 Ref-L0025N0752	25	$2 \times 752^3$	67.77	0.307	0.04825	0.693	$2.26 \times 10^5$	$1.21 \times 10^6$
EAGLE-3 Recal-L0025N0752	25	$2 \times 752^3$	67.77	0.307	0.04825	0.693	$2.26 \times 10^5$	$1.21 \times 10^6$

within  $10 \times$  the stellar half-mass radii of subhaloes being at least  $10 \times$  more massive in stars. NGC 1052 has an effective radius of 34 arcsec (Davies & Illingworth 1986) corresponding to a 3D deprojected half-light radius of 4.4 kpc by assuming  $D = 20$  Mpc and spherical geometry (Wolf et al. 2010). The statistically expected 3D separation between the observed NGC 1052 and DF2 galaxies is about 98 kpc. Note that this analysis also includes non-central subhaloes.

Secondly, the algorithm searches for substructure-corrected DF2-like subhaloes by following the description of van Dokkum et al. (2018b) according to which DF2 is located at a distance of  $D = 20.0$  Mpc. These subhaloes must have total-to-stellar mass ratios of  $M_{\text{total}}/M_* < 2$  estimated by Danieli et al. (2019), stellar half-mass radii of either  $R_{1/2} \leq 2.7$  kpc or  $R_{1/2} \geq 2.7$  kpc depending on which of these two criteria gives, at the end, the lowest number of DF2-like objects (as is done in standard probability calculations), and  $M_* = (4 \times 10^7 - 10^9) M_\odot$ . Since only the radial velocity of the observed DF2 dwarf galaxy (also for DF4) is known, one must take into account that this object can have an even higher 3D velocity, with the statistically expected 3D velocity being  $\sqrt{3}$  times larger than its radial velocity. Each pre-selected subhalo is weighted by the fraction of all sky directions in which the peculiar velocities of selected subhaloes exceed the observed radial peculiar velocity of DF2. The sum over all weights,  $w_{\text{eff}}$ , gives the actual effective number,  $N_{\text{eff}}$ , of pre-selected DF2-like subhaloes in the simulation box

$$N_{\text{eff}} \equiv \sum_i^N w_{\text{eff},i} \equiv \sum_i^N \max\left(0, 1 - \frac{v_{\text{DF2}}}{v_{\text{pec},i}}\right), \quad (1)$$

where  $N$  is the number of pre-selected DF2-like subhaloes,  $v_{\text{pec},i}$  is the magnitude of the peculiar velocity vector of the  $i$ -th subhalo wrt. the simulation box (i.e. CMB) and  $v_{\text{DF2}}$  is the observed distance-dependent radial peculiar velocity of DF2 given by

$$v_{\text{DF2}} = v_{\text{DF2,CMB}} - H_0 D. \quad (2)$$

Here,  $D$  is the distance of DF2 from Earth and  $v_{\text{DF2,CMB}}$  is the peculiar velocity of DF2 wrt. the CMB reference frame being

$$v_{\text{DF2,CMB}} = \langle v_{\text{GCs}} \rangle - v_{\text{corr}} \quad (3)$$

$$= \underbrace{\langle v_{\text{GCs}} \rangle}_{\text{DF2}} - \underbrace{(v_{\text{helio}} - v_{\text{CMB}})}_{\text{NGC 1052}}, \quad (4)$$

where  $\langle v_{\text{GCs}} \rangle \approx 1803 \text{ km s}^{-1}$  is the mean velocity of 10 GCs in DF2,<sup>3</sup>  $v_{\text{helio}}$  is the heliocentric peculiar velocity, and  $v_{\text{CMB}}$  is the peculiar velocity wrt. the CMB reference frame. The CMB rest-frame correction,  $v_{\text{corr}}$ , of DF2 is unknown and since DF2 has a similar sky position as NGC 1052,  $v_{\text{corr}}$  is calculated for NGC 1052 with  $v_{\text{helio}} = 1510 \pm 6 \text{ km s}^{-1}$  and  $v_{\text{CMB}} = 1293 \pm 16 \text{ km s}^{-1}$  taken from the NASA/IPAC Extragalactic Database<sup>4</sup> (Denicoló et al. 2005).

In the third step, the motion of DF2 wrt. the LG is quantified. The algorithm searches for all pre-selected DF2-like subhalo LG-like objects, which are defined for simplicity as subhaloes with  $M_* = 10^{10} - 10^{12} M_\odot$  and  $M_{200} = 10^{12} - 10^{13} M_\odot$  within a spherical shell with  $D \pm 1$  Mpc centred at the position of the pre-selected DF2-like subhalo. The line-of-sight velocity of the pre-selected DF2-like subhalo is

$$v_{\text{DF2,los}} = (v_{\text{pec}} \cdot \hat{\mathbf{r}}) \hat{\mathbf{r}}, \quad (5)$$

where  $v_{\text{pec}}$  is the velocity vector of the DF2-like subhalo and  $\hat{\mathbf{r}}$  is the normalized direction vector between an LG- and DF2-like galaxy. At  $D = 20.0$  Mpc, DF2 has a radial peculiar velocity of  $186 \text{ km s}^{-1}$  towards  $(l, b)_{\text{DF2}} = (182.02^\circ, -57.93^\circ)$ . DF4 has  $-173 \text{ km s}^{-1}$  towards  $(l, b)_{\text{DF4}} = (181.27^\circ, -58.18^\circ)$  and is thus moving towards us. The relative peculiar velocity between LG- and DF2-like subhaloes is given by

$$v_{\text{rel}} = |v_{\text{DF2,los}} - v_{\text{LG}}|, \quad (6)$$

where  $v_{\text{LG}}$  is the peculiar velocity of LG-like subhaloes. The LG moves with a peculiar velocity of  $v_{\text{LG}} = 627 \pm 22 \text{ km s}^{-1}$  wrt. the CMB frame towards  $(l, b)_{\text{LG}} = (276^\circ \pm 3^\circ, 30^\circ \pm 3^\circ)$  (Kogut et al. 1993). The angle between the normalized vectors  $\hat{\mathbf{v}}_{\text{DF2,los}}$  and  $\hat{\mathbf{v}}_{\text{LG}}$  is calculated by

$$\theta = \arccos(\hat{\mathbf{v}}_{\text{DF2,los}} \cdot \hat{\mathbf{v}}_{\text{LG}}), \quad (7)$$

<sup>3</sup> Emsellem et al. (2019) found a slightly lower mean velocity of the diffuse stellar body of  $1792.9_{+1.4}^{-1.8} \text{ km s}^{-1}$  compared to the mean velocity of 10 GCs derived by van Dokkum et al. (2018b).

<sup>4</sup> <https://ned.ipac.caltech.edu/>



and is distance-independent. The observed angle between the peculiar velocity vector of the LG and the radial velocity vector of DF2 is  $\theta = 117^\circ$ . A pre-selected DF2-like subhalo is finally counted as a real DF2-like object if at least one simulated LG-DF2-like pair is found which fulfills both  $v_{\text{rel}} \geq v_{\text{LG-DF2}}$  and  $\theta \geq 117^\circ$ , where  $v_{\text{LG-DF2}}$  is the observed relative velocity between the LG and DF2; otherwise the pre-selected DF2-like object is rejected and the effective number is reduced

$$N_{\text{eff}} \rightarrow N_{\text{eff}} - \sum_{j=1}^{N_{\text{rej}}} w_{\text{eff},j}, \quad (8)$$

where  $N_{\text{rej}}$  is the number of all rejected pre-selected DF2-like subhaloes. Note that this approach is designed to minimize possible tension with  $\Lambda$ CDM because only one such LG-DF2-like pair is needed for the subhalo to count as a DF2-like object. The probability of DF2-like subhaloes,  $p_{\text{DF2,sim}}$ , is then calculated by dividing the so-obtained effective number of DF2-like subhaloes by the number of substructure-corrected subhaloes within the stellar mass bin of  $M_* = (4 \times 10^7 - 10^9) M_\odot$ . The probability of DF4-like subhaloes,  $p_{\text{DF4,sim}}$ , is calculated in the same way. The structural probability of DF2-like subhaloes,  $p_{\text{DF2,structure}}$ , is obtained by selecting substructure-corrected subhaloes without any constraints on the peculiar velocity and motion to LG-like subhaloes. In order to isolate the effect of the peculiar velocity constraints, we compare the effective number of analogs before and after applying them. Therefore, we define the peculiar velocity probability by

$$p_{\text{DF2,vel}} \equiv \frac{p_{\text{DF2,sim}}}{p_{\text{DF2,structure}}}. \quad (9)$$

The analysis is repeated for different distances down to 10.0 Mpc with a resolution of  $\Delta D = 0.5$  Mpc but only for the description of Martin et al. (2018) in which  $M_{\text{total}}/M_* < 8.1$  at 20.0 Mpc is proposed in order to minimize tension with the  $\Lambda$ CDM model. The selection parameters  $M_*$ ,  $R_{1/2}$ ,  $M_{\text{total}}/M_*$ , and velocities are adjusted for different distances,  $D$ , via the scaling relations stated in Appendix A. In the Illustris-1, TNG100-1, and EAGLE-1 simulations  $M_* = 10^8 M_\odot$  corresponds to  $\gtrsim 50$  stellar particles. The two high-resolution runs of the EAGLE simulations (EAGLE-2 and EAGLE-3) are also used to study subhaloes with  $M_* = 10^7 M_\odot$  corresponding to  $\approx 40$  stellar particles (see also Table 1). We choose a large stellar mass bin for selected DF2-like subhaloes in order to include subhaloes with much more stellar particles, i.e. at 10.0 Mpc the upper end of the stellar mass bin is  $2.5 \times 10^8 M_\odot$ . We emphasize that DF2 has  $M_* = 2 \times 10^8 M_\odot$ , which is sufficiently resolved for the here applied analysis. A very detailed description of the resolution issues is available in Haslbauer et al. (2019). It would be difficult to extend our analysis to  $D < 10.0$  Mpc because the lower end of the stellar mass bin would be  $M_* < 10^7 M_\odot$ , making the resolution of subhaloes insufficient for the present analysis.

DF4-like subhaloes with  $M_{\text{total}}/M_* < 2$ , a  $R_{1/2}$  threshold of 2.0 kpc,  $M_* = (4 \times 10^7 - 10^9) M_\odot$ , and a mean radial velocity of the seven GCs of  $\langle v_{\text{GCs}} \rangle \approx 1446 \text{ km s}^{-1}$  are only analysed

at  $D = 20.0$  Mpc.<sup>5</sup> The selection criteria for DF2- and DF4-like galaxies scaled for different distances are summarized in Table 2.

### 3 RESULTS

We estimate the probability of detecting DF2- and DF4-like galaxies in the most modern cosmological  $\Lambda$ CDM simulations at redshift  $z = 0$ . The GC population in the observed DF2 dwarf galaxy is compared with that in the MW using the 2010 edition of the Harris (1996) catalogue.<sup>6</sup>

#### 3.1 DF2- and DF4-like galaxies in cosmological simulations

The structural probability of the occurrence of DF2-like subhaloes in dependence of distance, selected based on its structural properties and assuming the physical description of Martin et al. (2018), is shown in the left-hand panel of Fig. 1. The constraints on  $R_{1/2}$ ,  $M_*$ , and  $M_{\text{total}}/M_*$  cause a decrease of the frequency by about two orders of magnitude in the TNG100-1 simulation, in which the chance of finding such DF2-like galaxies becomes maximal at  $D = 11.5_{-1.5}^{+4.0}$  Mpc. The role of the structural properties is discussed in more detail in Section 4.1.1.

The right-hand panel of Fig. 1 reveals that, when the peculiar velocity is taken into account, the frequency of DF2-like subhaloes is reduced by another two orders of magnitude for  $D \lesssim 13$  Mpc and by about one order of magnitude for  $D \gtrsim 16$  Mpc. The peculiar velocity constraints alone prefer the maximal allowed distance of  $D = 20.0$  Mpc with a  $1\sigma$  ( $2\sigma$ ) lower distance limit of  $D = 16.5$  Mpc ( $D = 12.0$  Mpc). Had we allowed  $D > 20$  Mpc,  $p_{\text{vel}}$  would peak at an even larger distance – the Hubble flow distance is  $v_{\text{DF2,CMB}}/H_0 = 23$  Mpc. At a distance of 13.0 Mpc the observed DF2 galaxy would have a high peculiar velocity wrt. the CMB of  $v_{\text{pec}} \approx 676 \text{ km s}^{-1}$ , which differs from that of the LG by  $v_{\text{rel}} \approx 1112 \text{ km s}^{-1}$  with an angle of  $\theta = 117^\circ$ . About 13% of pre-selected DF2-LG-like systems fulfill the latter two constraints and according to Table 3 this fraction shows only a weak dependence with distance for the TNG300-1 simulation. Thus, the decrease of the frequency of DF2-like galaxies for smaller distance is generated by the peculiar velocity of DF2 wrt. the CMB reference frame.

The distance-dependent peculiar velocity probability is almost exactly the same for subhaloes in the TNG100-1 and TNG300-1, which is spatially three times larger than the former simulation run and includes therefore much more large-scale waves. This consistency between these two simulation runs could be either a pure coincidence or it means that the peculiar velocity field of DF2-like subhaloes has already converged in the TNG100-1 simulation. The convergence of the velocity fields of TNG100-1 and TNG300-1 are addressed in Section 4.1.2. Since TNG100-1 has a much better resolution than TNG300-1 (see Table 1) and the role of the peculiar

<sup>5</sup> The median radial velocity of the seven GCs of DF4 is  $1445 \text{ km s}^{-1}$ .

<sup>6</sup> [https://www.physics.mcmaster.ca/Fac\\_Harris/mwgc.dat](https://www.physics.mcmaster.ca/Fac_Harris/mwgc.dat)

**Table 2.** Selection criteria for DF2- and DF4-like galaxies in the cosmological simulations by placing the observed DF2 galaxy at different distances,  $D$ , from Earth. The properties at  $D = 20$  Mpc are scaled to smaller distances using the scaling relations in Appendix A.

References	obj.	$D$ [Mpc]	$M_{\text{total}}/M_*$	$M_*$ [ $M_{\odot}$ ]	$R_{1/2}$ [kpc]	$v_{\text{pec}}$ [ $\text{km s}^{-1}$ ]	$v_{\text{rel}}$ [ $\text{km s}^{-1}$ ]	$\theta$ [ $^{\circ}$ ]
van Dokkum et al. (2018b)	DF2	20	< 2	$4.0 \times 10^7$ to $1.0 \times 10^9$	2.7	$\geq 186$	$\geq 731$	$\geq 117$
Martin et al. (2018)	DF2	20	< 8.1	$4.0 \times 10^7$ to $1.0 \times 10^9$	2.7	$\geq 186$	$\geq 731$	$\geq 117$
–	DF2	16	< 10.1	$2.6 \times 10^7$ to $6.4 \times 10^8$	2.2	$\geq 466$	$\geq 936$	$\geq 117$
–	DF2	13	< 12.5	$1.7 \times 10^7$ to $4.2 \times 10^8$	1.8	$\geq 676$	$\geq 1112$	$\geq 117$
–	DF2	10	< 16.2	$1.0 \times 10^7$ to $2.5 \times 10^8$	1.4	$\geq 886$	$\geq 1298$	$\geq 117$
van Dokkum et al. (2019)	DF4	20	< 2	$4.0 \times 10^7$ to $1.0 \times 10^9$	2.0	$\geq 172$	$\geq 723$	$\geq 118$

**Table 3.** Fraction of pre-selected DF2 analogues for which an LG-like vantage point exists with  $v_{\text{rel}} \geq v_{\text{LG-DF2}}$  (Equation 6) and  $\theta \geq 117^{\circ}$  (Equation 7) for different adopted distances in the TNG300-1 simulation ( $D = 10, 13, 16, 20$  Mpc and  $v_{\text{LG-DF2}} = 1298, 1112, 936, 731 \text{ km s}^{-1}$ , respectively).

$D$ [Mpc]	$v_{\text{rel}} \geq v_{\text{LG-DF2}}$	$\theta \geq 117^{\circ}$	$\theta \geq 117^{\circ} \wedge v_{\text{rel}} \geq v_{\text{LG-DF2}}$
20	0.22	0.21	0.094
16	0.20	0.22	0.11
13	0.20	0.26	0.13
10	0.22	0.29	0.14

velocity is the same for both simulations, we use the former one for our main results.

The probability of DF2-like galaxies occurring in a  $\Lambda$ CDM cosmology evaluated by combining the structural and peculiar velocity constraints without considering its GC population is finally given in Fig. 2. The probability increases for a larger distance and becomes maximal for our allowed distance range in TNG100-1 with  $1.2 \times 10^{-3}$  at a distance of  $D = 20.0$  Mpc with a  $1\sigma$  ( $2\sigma$ ) lower distance limit of 16.0 Mpc (11.5 Mpc). The effective numbers, co-moving number densities, and probabilities of detecting DF2-like galaxies with  $M/L$  ratios consistent with Martin et al. (2018) for different distances and simulation runs are listed in Table 4.

By adopting the physical properties of both galaxies according to van Dokkum et al. (2018b, 2019) the maximal probability for finding each DF2- and DF4-like object is  $9.0 \times 10^{-5}$  (TNG100-1) and  $1.4 \times 10^{-4}$  (TNG300-1), respectively. That is, to find both at the same time has a probability of  $1.3 \times 10^{-8}$ . Therefore, in order to minimize the tensions with  $\Lambda$ CDM theory our main analysis relies on the description of Martin et al. (2018) according to which the  $M_{\text{total}}/M_*$  ratio is about four times larger than proposed by van Dokkum et al. (2018b). The effective numbers, co-moving number densities, and probabilities of DF2- and DF4-like galaxies assuming  $D = 20$  Mpc are summarized in Table 5.

Thus, applying the above-stated selection criteria (see Table 2) on the subhaloes of the Illustris-1, TNG100-1, TNG300-1, and EAGLE simulations shows that both DF2- and DF4-like galaxies are rare in  $\Lambda$ CDM simulations. Neither DF2 nor DF4 analogues can be found in the EAGLE-2 and EAGLE-3 simulations. In the following section we quantify the distance-dependent likelihood of the GC population and combine it with the probability obtained from the cosmological simulations.

### 3.2 Luminosities of globular clusters in DF2

The observed DF2 dwarf galaxy has unusually bright and large GCs if located at a distance of around 20 Mpc from Earth. This is notable, because up to now it is understood that all galaxies have a canonical peak of the GC luminosity distribution at  $M_V = -7.5$  (Rejkuba 2012). In contrast to that, van Dokkum et al. (2018c) estimate that DF2 has in total 15 GCs with absolute magnitudes  $M_{V,606} < -6.5$  and 11 of them are spectroscopically confirmed and have  $M_{V,606} \leq -8.6$ , therewith being much brighter than the expected canonical peak from other observed galaxies. This exceptional GC population poses the question if DF2 might be located at a much smaller distance from Earth, which will be addressed by the following statistical tests. We scale the luminosities of 15 GCs down to smaller distances and compare them with those of the MW<sup>7</sup> (Harris 1996) within the same luminosity ranges starting with  $M_{V,606} \leq -6.5$  at  $D = 20$  Mpc. The right and bottom panels of fig. 3 in van Dokkum et al. (2018c) show the observed interloper-corrected luminosity function of the compact objects (GCs) in DF2 according to which almost no additional GCs can be found in the  $-5 < M_{V,606} < -6.5$  range. This allows us to scale the magnitudes (and sizes) of the 15 GCs up to  $D = 10$  Mpc.

Since the magnitudes of the four GCs within  $-8.6 < M_{V,606} < -6.5$  are not reported in van Dokkum et al. (2018c), we assume that all of them have  $M_{V,606} = -7.5$  to minimize the tension with the GC population of other observed galaxies. The  $P$ -values of the following statistical tests on the GC luminosity distributions scaled for different distances are listed in Table 6.

#### 3.2.1 Binomial distribution

Given that observed quantities,  $X$ , are binomially distributed, which we symbolically express here by  $X \sim B(n, p)$ , the corresponding cumulative distribution function has the form

$$P(\geq k; p, n) \equiv P(X \geq k | X \sim B(n, p)) = \sum_{i=k}^n \binom{n}{i} p^i (1-p)^{n-i}, \quad (10)$$

<sup>7</sup> The Harris catalogue (Harris 1996) lists the absolute visual magnitudes of GCs in the MW which can be converted to the  $V_{606}$  band via  $M_{V,606} = M_V - 0.05$ .

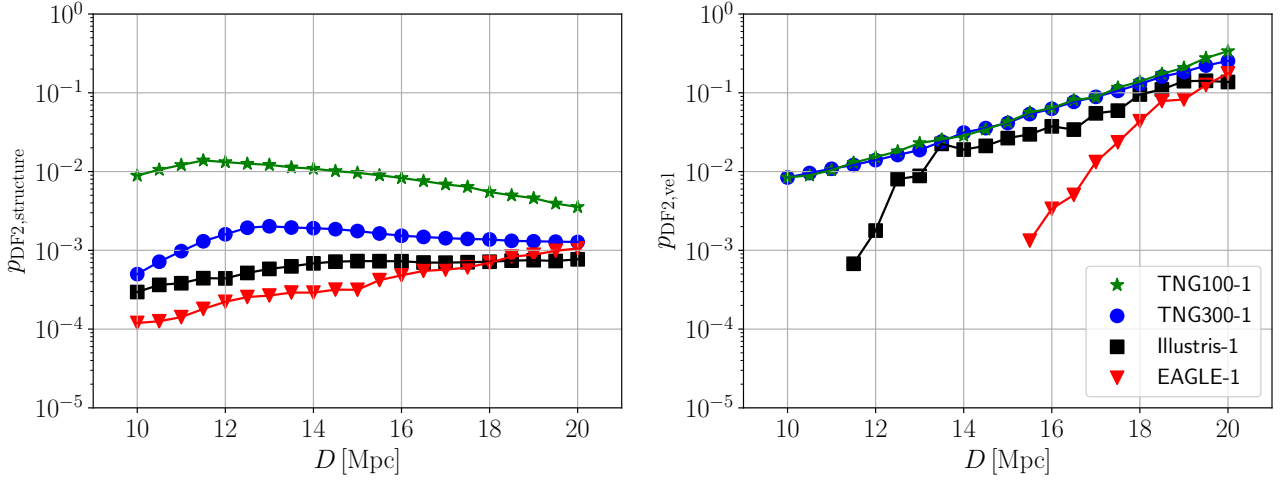


**Figure 1.** Left: Structural probability,  $p_{\text{DF2,structure}}$ , of DF2-like subhaloes over distance,  $D$ , in the Illustris-1 (black squares), TNG100-1 (green stars), TNG300-1 (blue dots), and EAGLE-1 (red triangles) simulations. We note that these probabilities only include the structural properties of DF2 and do not include its peculiar velocity and GC population. Right: Peculiar velocity probability,  $p_{\text{DF2,vel}}$  (Equation 9), of DF2-like subhaloes over distance.

**Table 4.** Effective number,  $N_{\text{DF2,eff}}$  (Equation 1 and Equation 8), effective co-moving number density,  $n_{\text{DF2,eff}}$ , and fraction of DF2-like galaxies,  $p_{\text{DF2,sim}}$ , in different simulation runs for different distances,  $D$ . The numbers in brackets give the unweighted number of DF2-like subhaloes,  $N_{\text{DF2}}$ . Here we assume  $M_{\text{total}}/M_*$  ratios consistent with Martin et al. (2018). The selection criteria for DF2- and DF4-like galaxies are listed in Table 2.

Distances	20 Mpc (Martin et al. 2018)			16 Mpc			13 Mpc			10 Mpc		
Simulation	$N_{\text{DF2,eff}}$ ( $N$ )	$n_{\text{DF2,eff}}$ [ $\text{cMpc}^{-3}$ ]	$p_{\text{DF2,sim}}$	$N_{\text{DF2,eff}}$ ( $N$ )	$n_{\text{DF2,eff}}$ [ $\text{cMpc}^{-3}$ ]	$p_{\text{DF2,sim}}$	$N_{\text{DF2,eff}}$ ( $N$ )	$n_{\text{DF2,eff}}$ [ $\text{cMpc}^{-3}$ ]	$p_{\text{DF2,sim}}$	$N_{\text{DF2,eff}}$ ( $N$ )	$n_{\text{DF2,eff}}$ [ $\text{cMpc}^{-3}$ ]	$p_{\text{DF2,sim}}$
Illustris-1	7.5 (12)	$6.2 \times 10^{-6}$	$1.1 \times 10^{-4}$	2.2 (5)	$1.8 \times 10^{-6}$	$2.7 \times 10^{-5}$	0.45 (2)	$3.7 \times 10^{-7}$	$5.1 \times 10^{-6}$	0 (0)	0	0
TNG100-1	52.0 (79)	$3.8 \times 10^{-5}$	$1.2 \times 10^{-3}$	26.2 (69)	$1.9 \times 10^{-5}$	$5.3 \times 10^{-4}$	15.7 (51)	$1.2 \times 10^{-5}$	$2.8 \times 10^{-4}$	5.1 (20)	$3.7 \times 10^{-6}$	$7.5 \times 10^{-5}$
TNG300-1	180.3 (275)	$6.5 \times 10^{-6}$	$3.2 \times 10^{-4}$	65.6 (163)	$2.4 \times 10^{-6}$	$9.6 \times 10^{-5}$	31.9 (102)	$1.2 \times 10^{-6}$	$3.8 \times 10^{-5}$	4.5 (15)	$1.6 \times 10^{-7}$	$4.2 \times 10^{-6}$
EAGLE-1	9.2 (16)	$9.2 \times 10^{-6}$	$1.9 \times 10^{-4}$	0.10 (1)	$1.0 \times 10^{-7}$	$1.6 \times 10^{-6}$	0 (0)	0	0	0 (0)	0	0
EAGLE-2	0 (0)	0	0	0 (0)	0	0	0 (0)	0	0	0 (0)	0	0
EAGLE-3	0 (0)	0	0	0 (0)	0	0	0 (0)	0	0	0 (0)	0	0

**Table 5.** Same as Table 4 but for DF2- and DF4-like galaxies if located at a distance of 20 Mpc. We assume for DF2 different  $M_{\text{total}}/M_*$  ratios (i.e.  $M_{\text{total}}/M_* < 8.1$  Martin et al. 2018 and  $M_{\text{total}}/M_* < 2$  van Dokkum et al. 2018b; see also Table 2).

References	20 Mpc (Martin et al. 2018)			20 Mpc (van Dokkum et al. 2018b)			20 Mpc (van Dokkum et al. 2019)		
Simulation	$N_{\text{DF2,eff}}$ ( $N$ )	$n_{\text{DF2,eff}}$ [ $\text{cMpc}^{-3}$ ]	$p_{\text{DF2,sim}}$	$N_{\text{DF2,eff}}$ ( $N$ )	$n_{\text{DF2,eff}}$ [ $\text{cMpc}^{-3}$ ]	$p_{\text{DF2,sim}}$	$N_{\text{DF4,eff}}$ ( $N$ )	$n_{\text{DF4,eff}}$ [ $\text{cMpc}^{-3}$ ]	$p_{\text{DF4,sim}}$
Illustris-1	7.5 (12)	$6.2 \times 10^{-6}$	$1.1 \times 10^{-4}$	2.9 (5)	$2.4 \times 10^{-6}$	$4.1 \times 10^{-5}$	3.1 (5)	$2.6 \times 10^{-6}$	$4.3 \times 10^{-5}$
TNG100-1	52.0 (79)	$3.8 \times 10^{-5}$	$1.2 \times 10^{-3}$	3.9 (6)	$2.9 \times 10^{-6}$	$9.0 \times 10^{-5}$	4.7 (7)	$3.5 \times 10^{-6}$	$1.1 \times 10^{-4}$
TNG300-1	180.3 (275)	$6.5 \times 10^{-6}$	$3.2 \times 10^{-4}$	13.8 (20)	$5.0 \times 10^{-7}$	$2.5 \times 10^{-5}$	80.2 (117)	$2.9 \times 10^{-6}$	$1.4 \times 10^{-4}$
EAGLE-1	9.2 (16)	$9.2 \times 10^{-6}$	$1.9 \times 10^{-4}$	0 (0)	0	0	0 (0)	0	0
EAGLE-2	0 (0)	0	0	0 (0)	0	0	0 (0)	0	0
EAGLE-3	0 (0)	0	0	0 (0)	0	0	0 (0)	0	0

where

$$\binom{n}{k} = \frac{n!}{k!(n-k)!} \quad (11)$$

is the binomial coefficient,  $n$  is the number of trials ( $n \in \mathbb{N}$ ),  $k$  is the number of successes ( $k \in [0, n]$ ), and  $p^k$  is the probability of having  $k$  successes ( $p \in [0, 1]$ ).

Assuming that the magnitudes of a GC population are binomially distributed, we consider two different approaches to quantify the differences between the GC populations of the MW and DF2. The first method (hereafter method 1) is sensitive to the medians of the GC magnitudes. We set  $p = 0.5$ ,  $n = 15$  (number of GCs in DF2), and  $k$  is the number of

DF2 GCs smaller or equal than the median of the magnitude of the GCs in the MW with  $M_{V,606} \leq -6.5$  if  $D = 20$  Mpc.

The second method (method 2) focuses more on the brightest GCs of the distribution. Here,  $p$  is the fraction of MW GCs with  $M_{V,606} \leq -8.6$  and  $M_{V,606} \leq -6.5$ ,  $n = 15$ , and  $k$  is the number of GCs in DF2 with  $M_{V,606} \leq -8.6$  if located at  $D = 20$  Mpc. Note that these magnitude thresholds are adopted for different distances with the scaling relation described in Appendix A.

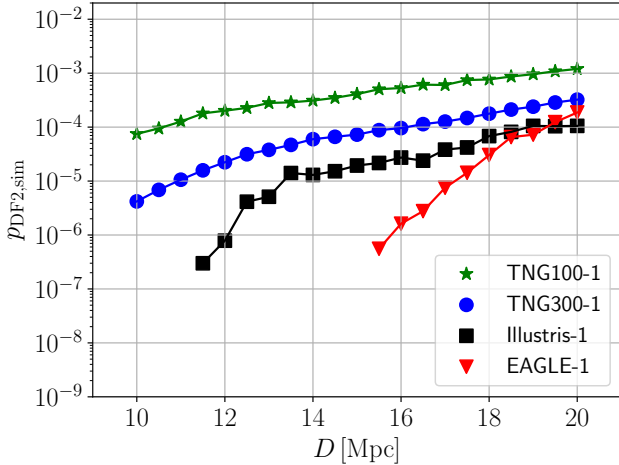


**Figure 2.** Cosmological detection probability,  $p_{\text{DF2, sim}}$ , in dependence of its distance,  $D$ , from Earth for the Illustris-1 (black squares), TNG100-1 (green stars), TNG300-1 (blue dots), and EAGLE-1 (red triangles) simulations. There are no DF2-like subhaloes in the EAGLE-2 and EAGLE-3 simulations.

### 3.2.2 Comparison of the means

The null hypothesis states that the means of two samples have to be the same. Since the Harris catalogue and table 1 in van Dokkum et al. (2018c) do not list the uncertainties of the GC magnitudes, we have to assume that the error on the mean of magnitudes of the MW GCs is zero and the uncertainty of the DF2 GCs is given by the intrinsic scatter of the MW GC population, i.e.  $\sigma_{\text{MW}}/\sqrt{N}$ , where  $N$  is the number of GCs in DF2 and  $\sigma_{\text{MW}}$  is the standard deviation of the magnitudes of the MW GCs.

In the case of two normal distributions, the standard score of the comparison of the means is then given by

$$Z = |\mu_{\text{DF2}} - \mu_{\text{MW}}| \div \frac{\sigma_{\text{MW}}}{\sqrt{N}}, \quad (12)$$

where  $\mu_{\text{MW}}$  and  $\mu_{\text{DF2}}$  are the means of the magnitudes of the MW and DF2 GCs. The two-tailed  $P$ -value is calculated by using a Gaussian distribution.

### 3.2.3 Mann–Whitney $U$ test

The Mann–Whitney  $U$  test (Mann & Whitney 1947), also known as the Wilcoxon 2-sample test (e.g. Kroupa 1995), is a non-parametric test, which compares the medians of two populations whereby the null hypothesis states that their medians are equal. The  $U$  test statistic for a two-tailed hypothesis is calculated by

$$U = \max(u_1, u_2), \quad (13)$$

with

$$u_1 = n_1 n_2 + \frac{n_1(n_1 + 1)}{2} - \sum_{i=1}^{n_1} r_{1,i}, \quad (14)$$

$$u_2 = n_1 n_2 - u_1, \quad (15)$$

where  $n_1$  and  $n_2$  are the sample sizes and  $r_1$  are the ranks of sample 1. If the samples are large enough we can assume that  $U$  follows a normal distribution, in which the standard score is obtained by

$$\mu = \frac{n_1 n_2}{2} + \underbrace{0.5}_C, \quad (16)$$

$$\sigma_{\text{corr}} = \sqrt{T_{\text{corr}} n_1 n_2 \left( \frac{n+1}{12} \right)}, \quad (17)$$

$$T_{\text{corr}} = 1 - \sum_{i=0}^k \left( \frac{t_i^3 - t_i}{n^3 - n} \right), \quad (18)$$

$$Z = \frac{U - \mu}{\sigma_{\text{corr}}}, \quad (19)$$

where  $n = n_1 + n_2$ ,  $C$  is a continuity correction,  $T_{\text{corr}}$  is the tie correction function,  $t_i$  is the number of subjects sharing rank  $i$ , and  $k$  is the number of tied ranks.

### 3.2.4 Kolmogorov–Smirnov test

The Kolmogorov–Smirnov (KS) test is also a non-parametric test comparing the cumulative probability distribution of two independent samples. The null hypothesis here is that the GC population of DF2 is drawn from that of the MW. The  $P$ -value is calculated by

$$m = \frac{n_1 n_2}{n_1 + n_2}, \quad (20)$$

$$\lambda = \left( \sqrt{m} + 0.12 + \frac{0.11}{\sqrt{m}} \right) D_{\text{max}}, \quad (21)$$

$$P = \sum_{i=1}^{\infty} (-1)^{i+1} \exp(-2\lambda^2 i^2), \quad (22)$$

where  $n_1$  and  $n_2$  are the numbers of the GCs in the MW and DF2, respectively, and  $D_{\text{max}}$  is the maximal difference in their cumulative probability distributions. The cumulative probability distributions of the GC magnitude distributions in the MW and DF2 scaled for different distances and their corresponding  $D_{\text{max}}$  values are presented in Fig. 3. Compared to the other above statistical test, the KS test is more sensitive to the whole GC population and is commonly used when the distributions of two samples have to be compared. Therefore, when calculating the combined probability of DF2 analogues in standard cosmology based on its occurrence in cosmological simulations and its GC population, the  $P$ -values of the KS test are used (see Section 3.5). The other tests (Sections 3.2.1–3.2.3) are applied as consistency checks.

## 3.3 Half-light radii of globular clusters in DF2

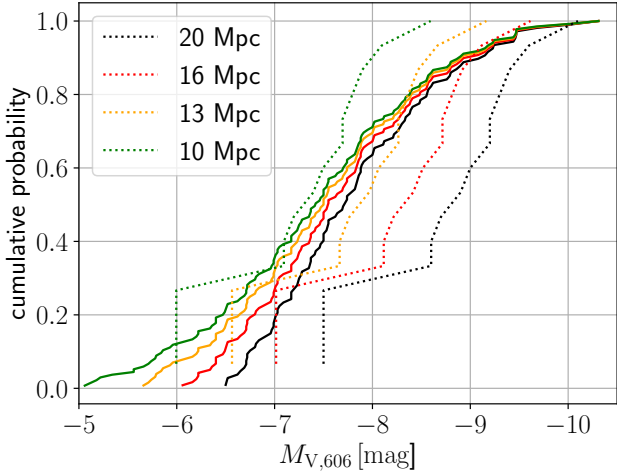
Here we apply the same statistical tests of Section 3.2 on the GC sizes but only to the 11 GCs with  $M_{V,606} \leq -8.6$  since for those the half-light radii and also their uncertainties are reported in van Dokkum et al. (2018c). Thus, at  $D = 20$  Mpc a luminosity range of  $M_{V,606} \leq -8.6$  is chosen, which scales to  $M_{V,606} \leq -7.1$  at 10 Mpc.

Fig. 4 presents the absolute magnitudes and sizes of GCs with  $M_{V,606} \leq -8.6$  in DF2 and DF4 if located at



**Table 6.**  $P$ -values of the binomial cumulative functions (see methods 1 and 2 in Section 3.2.1), comparison of the means (see Section 3.2.2), Mann–Whitney U test (see Section 3.2.3), and KS test (see Section 3.2.4) applied on the magnitude distribution of the GC population in the MW and DF2.

$D$ [Mpc]	$M_{V,606}$	$P$ -value (binomial 1)	$P$ -value (binomial 2)	$P$ -value (mean comp.)	$P$ -value (U-test)	$P$ -value (KS test)
20	$\leq -6.5$	$5.9 \times 10^{-2}$	$6.3 \times 10^{-6}$	$7.3 \times 10^{-5}$	$8.3 \times 10^{-4}$	$4.0 \times 10^{-4}$
16	$\leq -6.0$	$5.9 \times 10^{-2}$	$7.3 \times 10^{-4}$	$2.4 \times 10^{-2}$	$2.6 \times 10^{-2}$	$9.4 \times 10^{-3}$
13	$\leq -5.6$	$5.9 \times 10^{-2}$	$2.0 \times 10^{-2}$	$3.9 \times 10^{-1}$	$3.0 \times 10^{-1}$	$1.6 \times 10^{-1}$
10	$\leq -5.0$	$7.0 \times 10^{-1}$	$2.3 \times 10^{-1}$	$4.3 \times 10^{-1}$	$5.4 \times 10^{-1}$	$5.6 \times 10^{-1}$



**Figure 3.** Cumulative probability distributions of the GC magnitude distribution in the MW (solid lines) and DF2 (dashed lines). Different line colours refer to different distances of the observed DF2 galaxy from Earth (from left to right:  $D = 10$  Mpc, 13 Mpc, 16 Mpc, and 20 Mpc). The maximal differences between those two distributions are 0.21 ( $-8.1$  mag), 0.30 ( $-7.7$  mag), 0.43 ( $-8.1$  mag), and 0.55 ( $-8.6$  mag), respectively. Note that the four DF2 GCs with  $M_{V,606} > -8.6$  are assumed to have  $M_{V,606} = -7.5$ .

$D = 20$  Mpc. The properties of the DF2 GCs are scaled to smaller distances and compared with MW GCs within the same luminosity range. Table 7 summarizes the  $P$ -values of the statistical tests on the GC half-light radius distributions.

### 3.3.1 Binomial distribution

Same as method 1 in Section 3.2.1 with  $p = 0.5$  and  $n = 11$  by assuming that the GC sizes are binomially distributed.

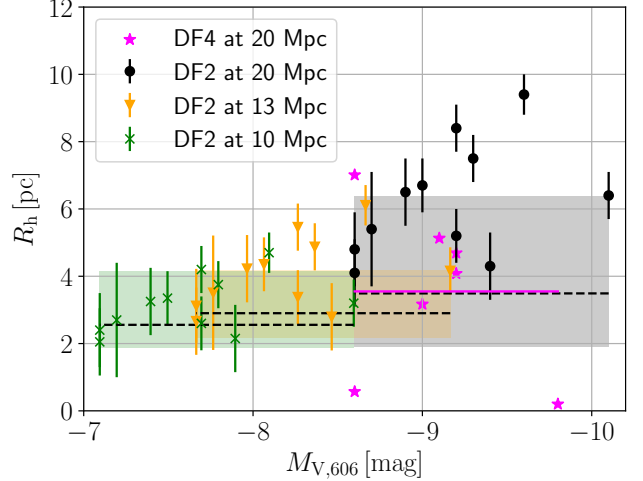
### 3.3.2 Comparison of the means

Table 1 in van Dokkum et al. (2018c) lists the uncertainties of the DF2 GC sizes. Thus, in contrast to Section 3.2.2 we have to use the inverse-variance weighted average

$$\sigma^2 = 1 \div \sum_i \frac{1}{(\sigma_i^2 + \sigma_{\text{MW}}^2)}, \quad (23)$$

$$\bar{\mu}_{\text{DF2}} = \sigma^2 \sum_i \frac{R_{h,i}}{(\sigma_i^2 + \sigma_{\text{MW}}^2)}, \quad (24)$$

where  $R_{h,i}$  and  $\sigma_i$  are the half-light radius and corresponding uncertainty of the  $i$ -th DF2 GC, and  $\sigma_{\text{MW}}$  is the standard



**Figure 4.** Circularized half-light radius,  $R_h$ , in dependence of the absolute magnitude,  $M_{V,606}$ , of GCs in DF2 and DF4 (magenta) with  $M_{V,606} \leq -8.6$  at 20 Mpc and scaled for different distances. The dashed horizontal lines mark the median of the half-light radii of GCs in the MW in the respective luminosity range and the shaded area marks the 16<sup>th</sup> and 84<sup>th</sup> percentile. The magenta solid line highlights the median of half-light radii of the seven GCs in DF4 (Danieli et al. 2019). The data points at 20 Mpc and errorbars are taken from van Dokkum et al. (2018c) (see table 1 and fig. 4).

deviation of the MW GC radii within the same luminosity range. Again, the standard score and the two-tailed  $P$ -value are evaluated.

### 3.3.3 Mann–Whitney U test

As in Section 3.2.3 but applied on the GC half-light radii.

### 3.3.4 Kolmogorov–Smirnov test

The cumulative probability distributions of the DF2 and MW GC half-light radius distributions and their maximum differences,  $D_{\text{max}}$ , are shown in Fig. 5.

## 3.4 GC probabilities

Summing up, all the here applied statistical tests have shown that scaling the GC luminosities and sizes of the DF2 dwarf galaxy to  $D \approx 10 - 13$  Mpc resolves the tension with the observed GC population of the MW which is known to be

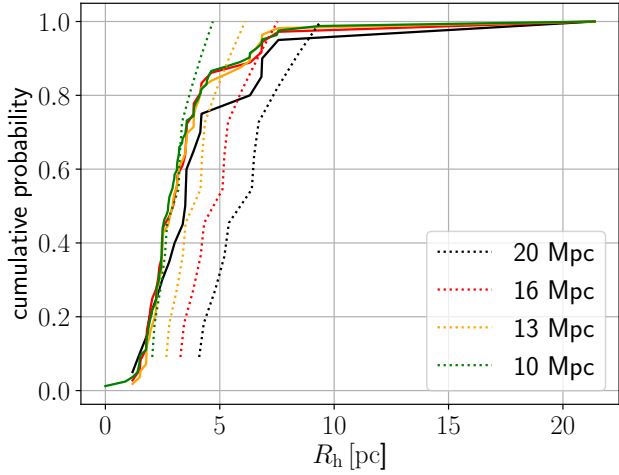


**Figure 5.** Cumulative probability distributions of the GC half-light radius distributions in the MW (solid lines) and DF2 (dashed lines). Different line colours refer to different distances of the observed DF2 galaxy from Earth (from left to right:  $D = 10$  Mpc, 13 Mpc, 16 Mpc, and 20 Mpc). The maximal differences between these distributions are 0.21 (2.0 pc), 0.43 (2.5 pc), 0.58 (3.2 pc), and 0.66 (4.2 pc), respectively.

representative (canonical; Rejkuba 2012). At  $D = 20$  Mpc the GC luminosity and half-light radius distributions of DF2 are in significant conflict with the GC population of the MW.

### 3.5 Combined cosmological and GC probability

In Section 3.1 we have shown that given its  $M_{\text{total}}/M_*$  value, stellar mass and half-mass radius, peculiar velocity, and motion relative to the LG,  $\Lambda$ CDM simulations favor that DF2 is located at a distance greater than 20 Mpc. In contrast, the above statistical tests applied on the GC population of DF2 in Sections 3.2 and 3.3 suggest much smaller distances of around 10 Mpc. Correlating in Fig. 6 the probabilities obtained from the cosmological simulations,  $p_{\text{DF2, sim}}$ , with the  $P$ -values of the KS test on the GC luminosity distribution (see Section 3.2.4) yields that the existence of such a dwarf galaxy is exceedingly rare in standard cosmology. Here we use the  $P$ -value of the KS test applied on the GC luminosity distribution, because this is statistically more robust than its GC half-light radius distribution compared to other galaxies (see last column of Tables 6 and 7). The probabilities globally peak at around 12 Mpc. Distances less than 10 Mpc are disfavoured by both the luminosity function and the other properties of DF2. This justifies our decision to not consider  $D < 10$  Mpc.

In Fig. 7 and Table 8 the combined probability,  $p_{\text{DF2, comb}}$ , is calculated by multiplying the probabilities from cosmological simulations,  $p_{\text{DF2, sim}}$ , with the  $P$ -values of the KS test by assuming that the GC population is independent of the structural properties of galaxies. The combined probability is maximal in the TNG100-1 simulation and peaks at a distance of  $11.5 \pm 1.5$  Mpc with  $1.0 \times 10^{-4}$  making the observed DF2 dwarf galaxy very unlikely in standard cosmology. This global peak is mainly driven by the GC population but is

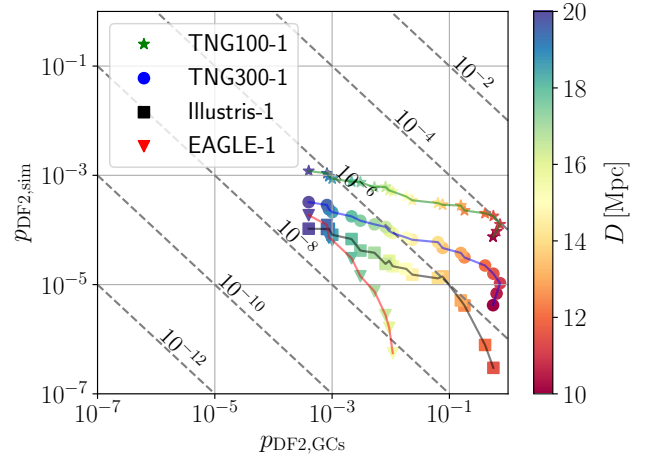


**Figure 6.** Cosmological detection probabilities of DF2-like dwarf galaxies obtained from all simulation runs,  $p_{\text{DF2, sim}}$ , (see also Table 4) and  $P$ -values of the KS test on the luminosity distribution of the observed DF2 galaxy,  $p_{\text{DF2, GCs}}$ , (see last column in Table 6) for different distances,  $D$ , represented by the colourbar. The dashed lines mark the positions of constant combined probability. The four different tracks belong to different simulations: Illustris-1 (squares, black line), TNG100-1 (stars, green line), TNG300-1 (dots, blue line), and EAGLE-1 (triangles, red line; see also the different sets in Fig. 7).

also apparent based on the structural properties (left-hand panel of Fig. 1).

NGC 1052 has a stellar mass of  $M_* \approx 10^{11} M_{\odot}$  (Forbes et al. 2017), which implies a host halo mass of  $M_{200} \approx 10^{13} M_{\odot}$ , and has a projected separation of 80 kpc from DF2 if located at  $D = 20$  Mpc. In Appendix B we show that restricting the analysis on DF2-like subhaloes embedded in host halos with  $M_{200} \leq 10^{13} M_{\odot}$  reduces the probabilities of DF2-like galaxies in the Illustris-1, TNG100-1, and TNG300-1 simulations by about one order of magnitude. DF2 then would be a  $4.6\sigma$  outlier within the  $\Lambda$ CDM framework.

## 4 DISCUSSION

Assuming that the standard model of cosmology is a correct description of the observed Universe, both dark-matter-dominated dwarf galaxies and TDGs void of dark matter must exist (Kroupa 2012; Haslbauer et al. 2019). Therefore the discovery of the two dark-matter-deficient galaxies DF2 and DF4 by van Dokkum et al. (2018b, 2019) are in principle consistent with the  $\Lambda$ CDM paradigm. Recently, Ploekinger et al. (2018) and Haslbauer et al. (2019) reported that dark-matter-free dwarf galaxies (i.e. tidal dwarf galaxy candidates) can be found in self-consistent cosmological simulations. However, based on the occurrence in cosmological simulations and the GC population of DF2, we have shown in this work that the chance of finding similar galaxies in standard cosmology is extremely low, with a maximal probability of  $1.0 \times 10^{-4}$  at a distance of  $D = 11.5 \pm 1.5$  Mpc obtained from the TNG100-1 simulation and assuming a  $M/L$  ratio consistent with Martin et al. (2018) (see Section 3.5).

**Table 7.**  $P$ -values of the binomial cumulative functions (see method 1 in Section 3.3.1), comparison of the means (see Section 3.3.2), Mann–Whitney U test (see Section 3.3.3), and KS test (see Section 3.3.4) applied on the half-light radius distribution of the GC population in the MW and DF2.

$D$ [Mpc]	$M_{V,606}$	$P$ -value (binomial 1)	$P$ -value (mean comp.)	$P$ -value (U-test)	$P$ -value (KS test)
20	$\leq -8.6$	$3.1 \times 10^{-5}$	$2.0 \times 10^{-1}$	$6.0 \times 10^{-2}$	$1.9 \times 10^{-3}$
16	$\leq -8.1$	$3.1 \times 10^{-5}$	$2.2 \times 10^{-1}$	$2.7 \times 10^{-3}$	$3.4 \times 10^{-3}$
13	$\leq -7.7$	$4.9 \times 10^{-4}$	$6.1 \times 10^{-1}$	$3.8 \times 10^{-2}$	$4.8 \times 10^{-2}$
10	$\leq -7.1$	$1.5 \times 10^{-1}$	$7.5 \times 10^{-1}$	$6.0 \times 10^{-1}$	$7.5 \times 10^{-1}$

**Table 8.** Combined probabilities,  $p_{\text{DF2,comb}}$ , of the existence of a DF2-like galaxy based on cosmological simulations and its GC population using the  $P$ -values of the KS test applied on the GC luminosity distribution (see Section 3.2.4 and last column of Table 6) for different distances (see also Figs 6 and 7).

Distances	20 Mpc (van Dokkum et al. 2018b)	20 Mpc (Martin et al. 2018)	16 Mpc	13 Mpc	10 Mpc
Simulation	$p_{\text{DF2,comb}}$	$p_{\text{DF2,comb}}$	$p_{\text{DF2,comb}}$	$p_{\text{DF2,comb}}$	$p_{\text{DF2,comb}}$
Illustris-1	$1.6 \times 10^{-8}$	$4.2 \times 10^{-8}$	$2.6 \times 10^{-7}$	$8.0 \times 10^{-7}$	0
TNG100-1	$3.6 \times 10^{-8}$	$4.8 \times 10^{-7}$	$5.0 \times 10^{-6}$	$4.4 \times 10^{-5}$	$4.2 \times 10^{-5}$
TNG300-1	$9.9 \times 10^{-9}$	$1.3 \times 10^{-7}$	$9.0 \times 10^{-7}$	$5.9 \times 10^{-6}$	$2.3 \times 10^{-6}$
EAGLE-1	0	$7.4 \times 10^{-8}$	$1.5 \times 10^{-8}$	0	0
EAGLE-2	0	0	0	0	0
EAGLE-3	0	0	0	0	0

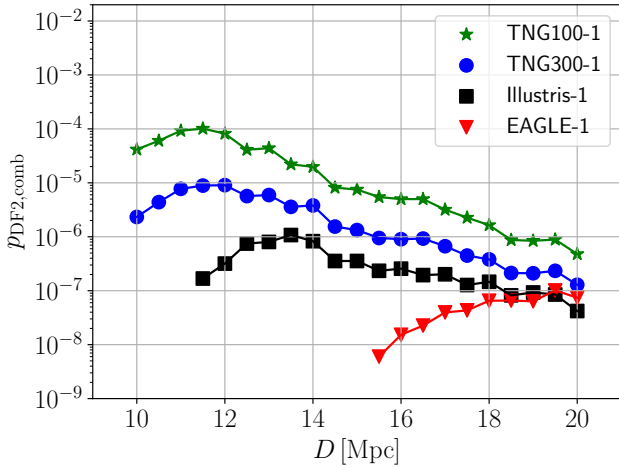


**Figure 7.** Combined probability of a DF2-like galaxy in standard cosmology,  $p_{\text{DF2,comb}}$ , in dependence of its distance,  $D$ , from Earth for the Illustris-1 (black squares), TNG100-1 (green stars), TNG300-1 (blue dots), and EAGLE-1 (red triangles) simulations (see also Table 8 for the absolute numbers). There are no DF2-like subhaloes in the EAGLE-2 and EAGLE-3 simulations. The combined probability,  $p_{\text{DF2,comb}}$ , is calculated by multiplying the probabilities from the  $\Lambda$ CDM simulations,  $p_{\text{DF2,sim}}$ , (see Table 4) with the  $P$ -values of the KS test on the GC luminosity populations.

It would be  $2.4 \times 10^{-5}$  at  $D = 11.0 \pm 0.5$  Mpc for the  $M/L$  ratio of van Dokkum et al. (2018b).

The probabilities in cosmological simulations are significantly reduced further if one focuses only on dark-matter-lacking galaxies embedded in host halos with  $M_{200} \leq 10^{13} M_{\odot}$  motivated by NGC 1052, which is in close location to DF2. This implies that such simulated galaxies are typi-

cally found in very massive galaxy clusters. Again, the highest probability is achieved in the TNG100-1 simulation with  $5.2 \times 10^{-6}$  at a slightly larger distance of  $13.0 \pm 1.5$  Mpc (see Appendix B). Such a distance is consistent with the work of Trujillo et al. (2019) in which they conclude that DF2 is located at  $D = 13.0 \pm 0.4$  Mpc based on redshift-independent distance indicators (see also fig. 18 in Trujillo et al. 2019).

In particular, without considering the unusual GC population, cosmological simulations suggest that DF2 is most likely located at a distance of  $D > 20$  Mpc from Earth. The probabilities of DF2-like galaxies with a dark matter content estimated from van Dokkum et al. (2018b) and Danieli et al. (2019) ( $M/L < 2 Y_{\odot}$ ) are about a factor of  $10 \times$  smaller than for galaxies with a slightly higher amount of dark matter as proposed by Martin et al. (2018) ( $M/L < 8.1 Y_{\odot}$ ). Thus, in order to minimize the tensions with  $\Lambda$ CDM cosmology, the analysis of the frequency of DF2 analogues over distance is taken here to rely on the description of Martin et al. (2018). In the following we discuss the role of the structural properties and peculiar velocity on the frequency of DF2-like subhaloes.

## 4.1 Comparison of simulations

### 4.1.1 Structural properties of subhaloes

According to the Dual Dwarf Theorem dark-matter-deficient galaxies are more compact than dark-matter-dominated galaxies (Kroupa et al. 2010; Dabringhausen & Kroupa 2013; Haslbauer et al. 2019). The observed DF2 galaxy is located, in the radius-mass-diagrams of the Illustris-1 simulation, almost exactly between dark-matter-poor and dark-matter-dominated galaxy branches (Haslbauer et al. 2019). That this cosmological simulation cannot reproduce the correct galaxy sizes of dark-matter-dominated galaxies (compared to observed galaxies) causes in the first place the low detec-

tion probabilities of DF2-like objects in the Illustris-1 simulation. The untypical stellar half-mass radii of simulated galaxies could be related to the implemented feedback models in the here analysed simulations. We have used the most modern self-consistent cosmological simulations, which rely on different feedback descriptions, galaxy evolution models, and different computer codes. The higher probabilities (Tables 4 and 5) of DF2-like galaxies in TNG100-1 and TNG300-1 can be explained by the fact that the TNG simulation produces stellar half-mass radii about  $2\times$  smaller than in the Illustris simulations for galaxies with  $M_* < 10^{10} M_\odot$  (Pillepich et al. 2018a).

The sizes of subhaloes are studied in Fig. 8 in which the radius- $M_{\text{total}}/M_*$  diagrams for substructure-corrected subhaloes with  $10^7 < M_*/M_\odot < 10^9$  in the here used simulation runs and the position of DF2 scaled for different distances (red stars) are plotted. Extracting the bin values along this locus of possible DF2 positions gives a distance-dependent probability distribution as shown in Fig. 9. The frequency of simulated DF2 analogues in the TNG100-1, TNG300-1, and EAGLE runs peaks between  $D = 13 - 20$  Mpc. In contrast, the frequency of Illustris-1 DF2 analogues increases for larger distances because subhaloes in the Illustris-1 simulation are typically less compact than in the other simulations and scaling DF2 to larger distances increases its half-light radius (see also the scaling relations in Appendix A). According to the TNG100-1 radius- $M_{\text{total}}/M_*$  contour diagram (upper right panel of Fig. 8), which does not consider the peculiar velocity and GC population, DF2 is at a  $2.0\sigma$  ( $D = 20$  Mpc),  $2.1\sigma$  ( $D = 16$  Mpc),  $2.3\sigma$  ( $D = 13$  Mpc), and  $2.5\sigma$  ( $D = 10$  Mpc) tension level with  $\Lambda$ CDM cosmology. This method, which quantifies the tension with  $\Lambda$ CDM by using contour plots, differs from that of our main analysis in which we calculated the structural probabilities by using the area of a rectangular defined by  $R_{1/2}$  and  $M_{\text{total}}/M_*$  scaled for different distances (see Table 2). The so-calculated structural probability of DF2-like subhaloes in dependence of its distance (see left-hand panel of Fig. 1) shows that the probability becomes maximal for the TNG100-1 simulation. Applying selection criteria for  $R_{1/2}$ ,  $M_*$ , and  $M_{\text{total}}/M_*$  causes a decrease in the number of subhaloes by about two orders of magnitude. The frequency of such DF2-like subhaloes is about  $10\times$  lower in the TNG300-1 simulation compared to TNG100-1. This can be caused either by the higher resolution of TNG100-1 or it means that the frequency of selected subhaloes in TNG100-1 has not converged since the box size of TNG100-1 is by a factor of  $3\times$  smaller than TNG300-1.

Using the Illustris-1 Yu et al. (submitted) find a large population of simulated dwarf galaxies with  $M_* < 5\times 10^8 M_\odot$  and  $M_{\text{dm}}/M_* < 0.1$  (see their Fig. 3). However, their analysis does not include any constraints on the sizes, environment, and peculiar velocity of dark-matter-lacking subhaloes. The role of the peculiar velocity is discussed in the following section.

#### 4.1.2 Velocity field of subhaloes

The analysis of simulated DF2 analogues is based on simulation runs with different computational box sizes. Small simulation boxes have a lack of large-scale waves, which affects the peculiar velocities in two ways. First, cosmological simulations do not have bulk velocities relative to the CMB.

Secondly, the absence of large-scale waves causes a lack of large-scale fluctuations and thus massive clusters. Therefore, peculiar velocities of subhaloes in small simulation boxes, like the Illustris-1, TNG100-1, and EAGLE runs, are not representative of a “real”  $\Lambda$ CDM Universe.

In order to address the lack of large-scale waves/fluctuations in cosmological simulations, we also used the TNG300-1 simulation which is the largest run of the IllustrisTNG project with a co-moving box size of  $L = 302.6$  cMpc. The LG moves with a peculiar velocity of about  $627 \text{ km s}^{-1}$  wrt. the CMB rest frame, which is most likely caused by the Shapely supercluster and the GA. Assuming that a large-scale structure causes a peculiar velocity of  $v_{\text{pec}} = 627 \text{ km s}^{-1}$  in the region of the LG, we estimate its maximal induced peculiar velocity  $\Delta v_{\text{pec}}$  on the motion of DF2 if such a supposed large-scale structure is just outside of the simulation box by

$$\Delta v_{\text{pec}} = \left(\frac{2D}{L}\right)v_{\text{pec}}. \quad (25)$$

The factor  $2/L$  takes into account that the LG-like structure is located in the middle of the simulation box and that the large-scale structure is exactly at the edge of the simulation box, which would be the worst situation for our analysis since it maximizes  $\Delta v_{\text{pec}}$ .  $D$  is again the distance between the LG and DF2.

The maximum induced peculiar velocity raised by the tides of a massive large-scale structure outside the simulation box would be rather small for the TNG300-1 simulation (i.e.  $\Delta v_{\text{pec}} = 54 \text{ km s}^{-1}$  for  $D = 13$  Mpc and  $\Delta v_{\text{pec}} = 83 \text{ km s}^{-1}$  for  $D = 20$  Mpc), but is significantly larger for the Illustris-1, TNG100-1, and EAGLE simulations (i.e. for the TNG100-1 simulation one gets:  $\Delta v_{\text{pec}} = 147 \text{ km s}^{-1}$  for  $D = 13$  Mpc and  $\Delta v_{\text{pec}} = 227 \text{ km s}^{-1}$  for  $D = 20$  Mpc).

Since the simulation box of TNG300-1 is much larger than those of the other simulations, it includes also much longer wave lengths resulting in a shift of the mode of the peculiar velocity field to higher values as seen in Table 9 and Fig. 10. In addition, we compare the velocity field of the TNG100-1 and TNG300-1 with the much larger Millennium simulation. The Millennium simulation is an  $N$ -body simulation carried out in a cosmological box with a length of  $L = 684.9$  cMpc based on a flat  $\Lambda$ CDM cosmology with  $\Omega_{\text{m}} = 0.25$ ,  $\Omega_{\text{b}} = 0.045$ ,  $\Omega_{\Lambda} = 0.75$ ,  $h = 0.73$ ,  $n = 1$ , and  $\sigma_8 = 0.9$  (Springel et al. 2005). Here we use the subhalo catalogue generated with the semi-analytical model from De Lucia et al. (2006). Due to the large box size of the Millennium simulation, one can assume that it is a very accurate representation of a  $\Lambda$ CDM Universe. According to Table 9 and Fig. 10 the velocity field of TNG300-1 is comparable with that of the Millennium simulation, i.e. the modes of the peculiar velocity of subhaloes are very similar for different stellar mass ranges and the standard binomial uncertainties of the velocity fields are very small. Thus, we can conclude that the velocity field has almost converged in the TNG300-1 simulation. Interestingly, the frequency of subhaloes with  $v_{\text{pec}} \approx 780 \text{ km s}^{-1}$  is slightly higher in the TNG300-1 compared to the Millennium simulation. The cross-over between the TNG100-1 and Millennium simulations happens at  $v_{\text{pec}} \approx 890 \text{ km s}^{-1}$ . Therefore, TNG300-1 (and also TNG100-1) can be safely used in order to address



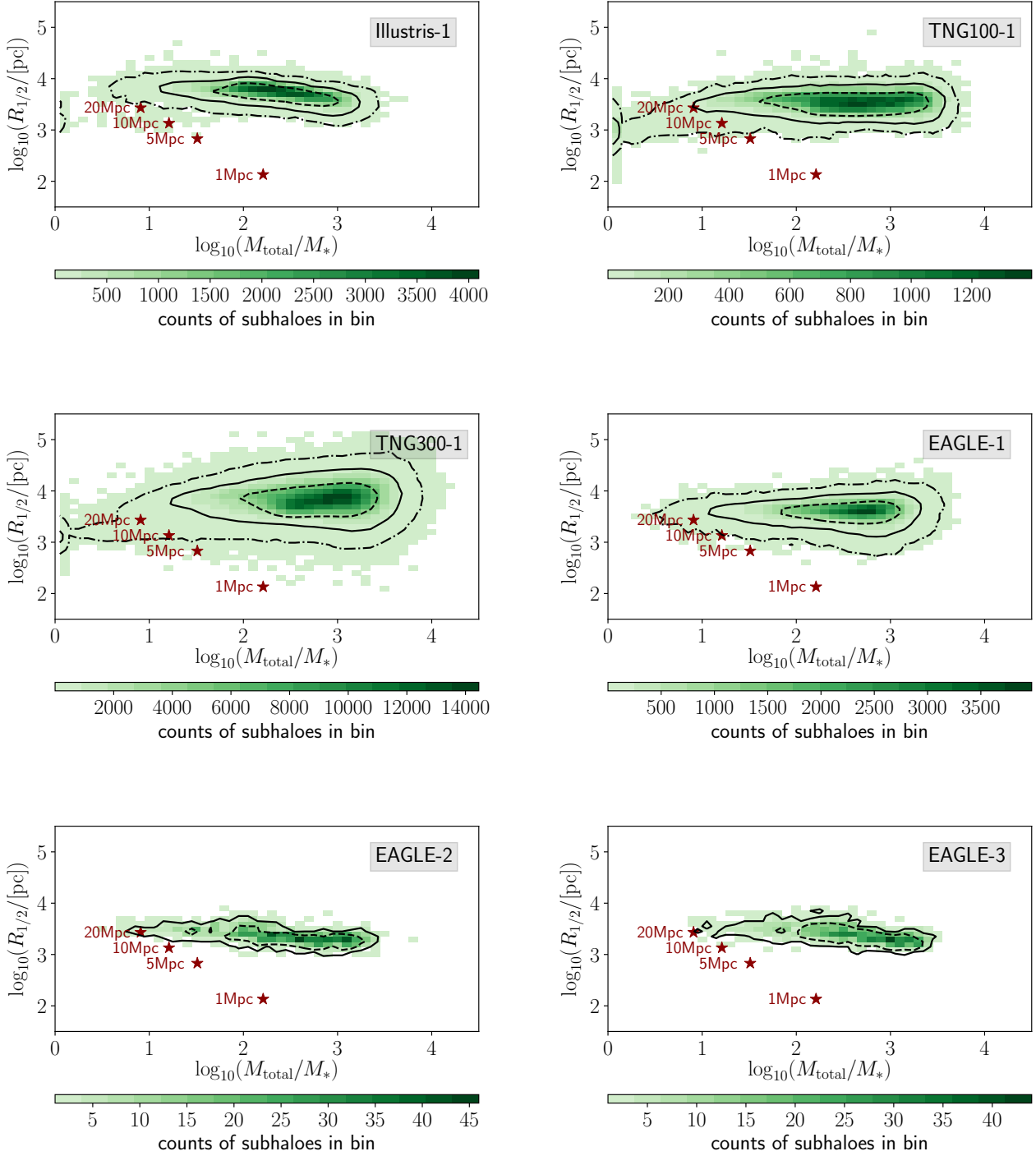


**Figure 8.** Radius- $M_{\text{total}}/M_*$  diagram for substructure-corrected subhaloes with  $10^7 < M_*/M_{\odot} < 10^9$  in the Illustris-1, TNG100-1, TNG300-1, EAGLE-1, EAGLE-2, and EAGLE-3 simulations. The distance-dependent probability density of simulated DF2 analogues (highlighted by red stars) is analysed in Fig. 9. The black lines mark the 1 $\sigma$  (dashed), 2 $\sigma$  (solid), and 3 $\sigma$  (long-dashed) confidence levels if shown. Using the contour plot of the TNG100-1 simulation (upper right panel), the structural properties of DF2 are in tension with  $\Lambda$ CDM cosmology at the 2.0 $\sigma$  ( $D = 20$  Mpc), 2.1 $\sigma$  ( $D = 16$  Mpc), 2.3 $\sigma$  ( $D = 13$  Mpc), and 2.5 $\sigma$  ( $D = 10$  Mpc) level.

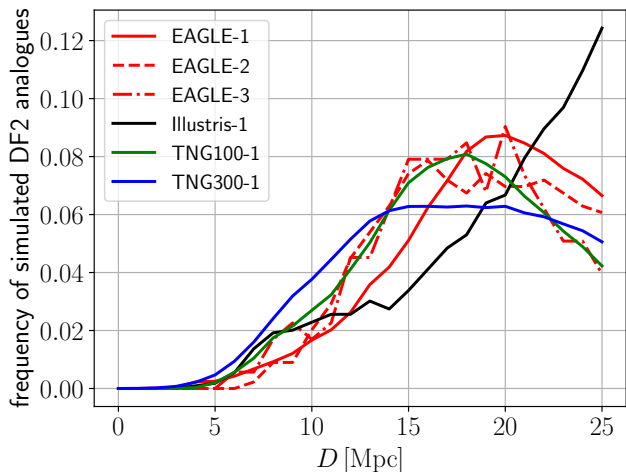


**Figure 9.** Distance-dependent probability density of DF2 analogues in the Illustris-1 (black), TNG100-1 (green), TNG300-1 (blue), and EAGLE (red) simulations with  $10^7 < M_*/M_\odot < 10^9$  calculated by extracting all bin values along the locus of possible DF2 positions in the radius- $M_{\text{total}}/M_*$  diagrams of Fig. 8 (highlighted by red stars).

the high peculiar velocity of DF2 which arises at a small distance. In particular, DF2 has  $v_{\text{pec}} = 780 \text{ km s}^{-1}$  at a distance of  $D = 11.5 \text{ Mpc}$  from Earth.

The role of the peculiar velocity on the detection probabilities of DF2-like subhaloes for different simulation runs was studied in Section 3.1 (right-hand panel of Fig. 1). At  $D = 20 \text{ Mpc}$ , the constraints on the peculiar velocity reduce their frequency in the TNG100-1 and TNG300-1 by a factor of 5 – 10. This factor increases for smaller distances and at  $D = 10 \text{ Mpc}$  the peculiar velocity conditions cause a drop in the frequency of at least two orders of magnitude. Interestingly, this effect is almost the same for the TNG100-1 and TNG300-1 simulation. This can be also just a coincidence. Since TNG100-1 has a better resolution than TNG300-1 (see Table 1) and the fact that the effect on the peculiar velocity is almost the same for both simulations, the main results of our analysis rely on TNG100-1.

We have shown that at a distance  $D \approx 10 - 13 \text{ Mpc}$  the peculiar velocity wrt. the CMB of the observed DF2 would be unusually high. But such high peculiar velocities do arise in the observed Universe. For example, the galaxies NGC 1400 and NGC 1407 have a difference in velocity relative to the Hubble flow of about  $1100 - 1200 \text{ km s}^{-1}$  (Spolaor et al. 2008; Tully 2015) and are probably within at least  $0.1 \text{ Mpc}$  of each other but the relative distance uncertainties are about  $4 \text{ Mpc}$  (see table 2 in Spolaor et al. 2008). Pawlowski & McGaugh (2014) reported that the NGC 3109 association forms a thin planar structure consisting of the galaxies Antila, NGC 3109, Sextans A, Sextans B, Leo P and suggested that the velocity with which this plane (which is parallel to one of the LG non-satellite galaxy planes situated symmetrically about the Milky Way-Andromeda line as discovered by Pawlowski et al. 2013) is moving away from the LG is too high for a  $\Lambda\text{CDM}$  cosmology (the backsplash problem). Detailed modelling of the LG has shown that such a high velocity of a planar structure is indeed in conflict with

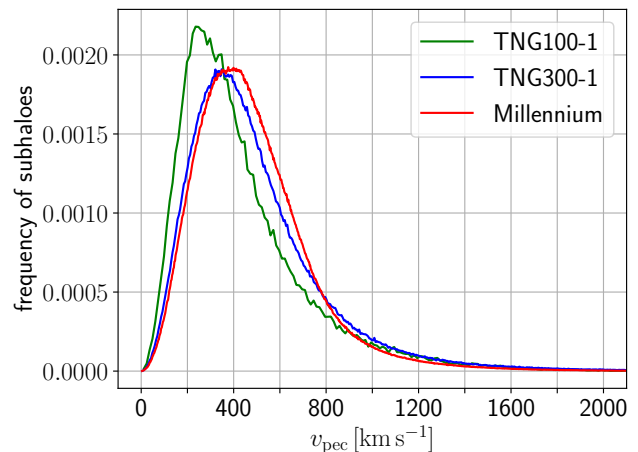


**Figure 10.** Peculiar velocity field at redshift  $z = 0$  of subhaloes with  $M_* > 10^7 M_\odot$  in the TNG100-1 (green;  $L = 110.7 \text{ cMpc}$ ), TNG300-1 (blue;  $L = 302.6 \text{ cMpc}$ ), and Millennium simulation (red;  $L = 684.9 \text{ cMpc}$ , Springel et al. 2005; De Lucia et al. 2006). The distributions for different stellar mass cuts are analysed in more detail in Table 9.

**Table 9.** Fraction of subhaloes with  $v_{\text{pec}} \geq 627 \text{ km s}^{-1}$  and the mode of the  $v_{\text{pec}}$  distribution in the TNG100-1 ( $L = 110.7 \text{ cMpc}$ ), TNG300-1 ( $L = 302.6 \text{ cMpc}$ ), and Millennium simulation ( $L = 684.9 \text{ cMpc}$ , Springel et al. 2005; De Lucia et al. 2006). We calculate standard binomial uncertainties by  $\sqrt{p(1-p)/n}$ , where  $p$  is the fraction of subhaloes with  $v_{\text{pec}} \geq 627 \text{ km s}^{-1}$  and  $n$  is the total number of subhaloes of the distribution. These uncertainties are always smaller than 0.005. The uncertainties of the velocity peaks are estimated by the chosen bin sizes of the histograms and the velocity fields are shown in Fig. 10.

$M_* [M_\odot]$	TNG100-1	TNG300-1	Millennium
$> 10^7$	0.185 $254 \pm 20 \text{ km s}^{-1}$	0.236 $351 \pm 20 \text{ km s}^{-1}$	0.220 $392 \pm 20 \text{ km s}^{-1}$
$10^7 - 10^9$	0.185 $254 \pm 20 \text{ km s}^{-1}$	0.233 $351 \pm 20 \text{ km s}^{-1}$	0.203 $352 \pm 20 \text{ km s}^{-1}$
$10^{10} - 10^{12}$	0.185 $255 \pm 20 \text{ km s}^{-1}$	0.250 $355 \pm 20 \text{ km s}^{-1}$	0.275 $416 \pm 25 \text{ km s}^{-1}$

the standard model of cosmology (Banik & Zhao 2017; Peebles submitted). On larger scales high velocities are also observed, for example in massive interacting galaxy clusters. The two dark matter peaks of the Bullet Cluster (1E0657-65) have a relative velocity of  $\approx 3000 \text{ km s}^{-1}$  (Kraljic & Sarkar 2015). Using FLASH-based  $N$ -body/hydrodynamical models Molnar & Broadhurst (2015) demonstrated that a pre-fall relative velocity of  $2250 \text{ km s}^{-1}$  is required to reproduce the observational parameters of the galaxy cluster El Gordo (ACT-CT J0102-4915). The tension with standard  $\Lambda\text{CDM}$  cosmology arises in that an initially homogeneous and isotropic Universe needs to produce bound structures which attain such high observed relative velocities within a Hubble time. This might be alleviated in MOND cosmology, where the impact velocity of the Bullet Cluster is not problematic (Angus & McGaugh 2008).

Interestingly, if DF2 is located at  $D = 13 \text{ Mpc}$ , its re-

sulting high peculiar velocity arises rather naturally in a MOND cosmology in which the law of gravity becomes non-Newtonian for accelerations  $\lesssim 10^{-10} \text{ ms}^{-2}$  (Milgrom 1983). The velocity field of halos is shown in Fig. 11 for the TNG300-1  $\Lambda$ CDM and cosmological MOND simulations conducted by Candlish (2016). We note that the distributions of the peculiar velocity of subhaloes and halos are very similar in  $\Lambda$ CDM simulations such that we assume here that the initial velocity fields of the halos and subhaloes in both the  $\Lambda$ CDM and MOND simulations are basically the same. In MOND cosmology the distribution of the present-day velocity field is shifted to higher values peaking around  $700 \text{ km s}^{-1}$  compared to that obtained from standard cosmology, which peaks at around  $250 \text{ km s}^{-1}$ . Remarkable is that the peculiar velocity of the LG ( $v_{\text{pec}} = 627 \pm 22 \text{ km s}^{-1}$ , Kogut et al. 1993) is well consistent with the position of the peak of the MONDian velocity distribution. At  $D = 13 \text{ Mpc}$ , the most likely peculiar velocity of DF2 is  $v_{\text{pec}} = 1171 \text{ km s}^{-1}$  and is likely in the case of MOND. In particular, about 1.9% of all subhaloes in the TNG300-1 simulation have  $v_{\text{pec}} \geq 1171 \text{ km s}^{-1}$ . In  $\Lambda$ CDM simulations the tails of the velocity distributions of subhaloes and halos are slightly different, because subhaloes can be boosted much easier to higher velocities. Thus, only 0.81% of all halos have  $v_{\text{pec}} \geq 1171 \text{ km s}^{-1}$  in the TNG300-1 simulation. In the two MOND versions AQUAL (Bekenstein & Milgrom 1984) and QUMOND (Milgrom 1983) about 4.2% and 4.7% of the halos have  $v_{\text{pec}} \geq 1171 \text{ km s}^{-1}$ , respectively. The MONDian simulations are carried out in a co-moving box size of only  $L \approx 46 \text{ cMpc}$  (Candlish 2016) and thus their velocity fields are not really representative of a “real” MONDian Universe due to a lack of large-scale waves/fluctuations. For reasons not related to technical problems, no self-consistent hydrodynamical cosmological simulation exists, which would allow a more detailed and quantitative comparison of the structural parameters of MONDian dwarf galaxies with DF2.

In the case of distances  $D \leq 13 \text{ Mpc}$ , a further challenge for  $\Lambda$ CDM is the large radial peculiar velocity of DF2 relative to the motion of the LG with a large angle between their velocity vectors at the same time (see also Table 3 in Section 3.1). Given that most of the peculiar velocity of the LG arises from the GA, one would expect that the velocity vectors of two such close and fast-moving galaxies like DF2 and the LG would point at least roughly in the same direction. Indeed, the combination of a large peculiar velocity and angle between their velocity vectors reduces the detection of LG-DF2-like pairs in cosmological simulations at lower distances from the Earth.

## 4.2 Comparison with observations

### 4.2.1 Observational constraints on the distance of DF2

At a distance of  $D = 20 \text{ Mpc}$ , DF2 and possibly also DF4 have an unusual GC population (van Dokkum et al. 2018b, 2019). A detailed comparison with the GC population of the MW with that of DF2 shows that the tension can be solved if DF2 is located at a much smaller distance of  $D \leq 13 \text{ Mpc}$ , which is in agreement with the findings by Trujillo et al. (2019) (see also Sections 3.2 and 3.3).

In contrast, van Dokkum et al. (2018d) argue that based on the radial peculiar velocity, projected sky-position, and

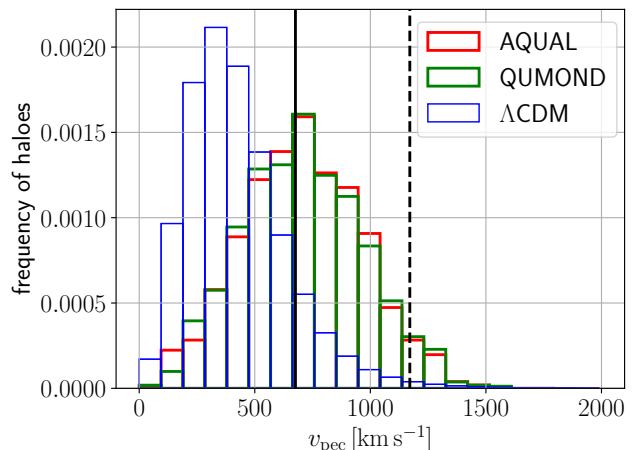


**Figure 11.** Peculiar velocity distribution of halos in  $\Lambda$ CDM (TNG300-1,  $L = 302.6 \text{ cMpc}$ ) and MOND cosmologies ( $L = 45.7 \text{ cMpc}$ ) using its traditional formulation as AQUAL (Bekenstein & Milgrom 1984) and the more computer-friendly QUMOND (Milgrom 2010). The distribution of the TNG300-1 velocity field is similar to the Newtonian case shown in Candlish (2016). The solid vertical line at  $v_{\text{pec}} = 676 \text{ km s}^{-1}$  marks the smallest possible peculiar velocity and the dashed line with  $\sqrt{3} \times$  as much ( $v_{\text{pec}} = 1171 \text{ km s}^{-1}$ ) highlights the most likely peculiar velocity of the observed DF2 dwarf galaxy if located at a distance of  $13 \text{ Mpc}$  from Earth. In the TNG300-1 simulation 1.9% of all subhaloes and 0.81% of all halos have  $v_{\text{pec}} \geq 1171 \text{ km s}^{-1}$ . In AQUAL and QUMOND 4.2% and 4.7% of the halos have  $v_{\text{pec}} \geq 1171 \text{ km s}^{-1}$ , respectively. The data for the MONDian cosmology are taken from Candlish (2016) (see right panel of Fig. 14).

SBF method DF2 has to be located at  $D = 19.0 \pm 1.7 \text{ Mpc}$  and due to the non-detection of red giant branch stars one can rule out a distance of  $D = 13 \text{ Mpc}$ . However, Trujillo et al. (2019) were able to identify the TRGB in the HST data from which they derived a distance of  $D = 13.4 \pm 1.1 \text{ Mpc}$ . In the framework of the IGIMF theory (Kroupa & Weidner 2003; Jeřábková et al. 2018) the SBF method would predict a lower distance compared to van Dokkum et al. (2018d). This is because the lower SFR of a dwarf galaxy results in a top-light IMF compared to more massive galaxies as quantified by Zonoozi et al. (in prep).

### 4.2.2 Comparison with other dwarf galaxies

We compare in Fig. 12 (left-hand panel) the position of DF2 with observed early-type galaxies from Dabringhausen & Fellhauer (2016) in the radius–mass plane. Restricting the sample to galaxies with  $M_* < 10^9 M_\odot$  gives that DF2 is consistent with observations at a  $(11 \pm 3)\%$  confidence level if located at  $D = 20 \text{ Mpc}$ . The radius–mass diagram also shows the position of DF2 scaled for different distances (red stars). Extracting the probability density of observed galaxies with  $M_* < 10^9 M_\odot$  along this locus (right-hand panel of Fig. 12) underpins that DF2 is, based on its size and stellar mass, not an exception compared to other observed galaxies and suggests that DF2 is statistically most likely at a distance of  $D = 6 \text{ Mpc}$ . Note that the sample of Dabringhausen & Fellhauer (2016) also includes a substantial number of galaxies with a surface brightness lower than that of DF2.

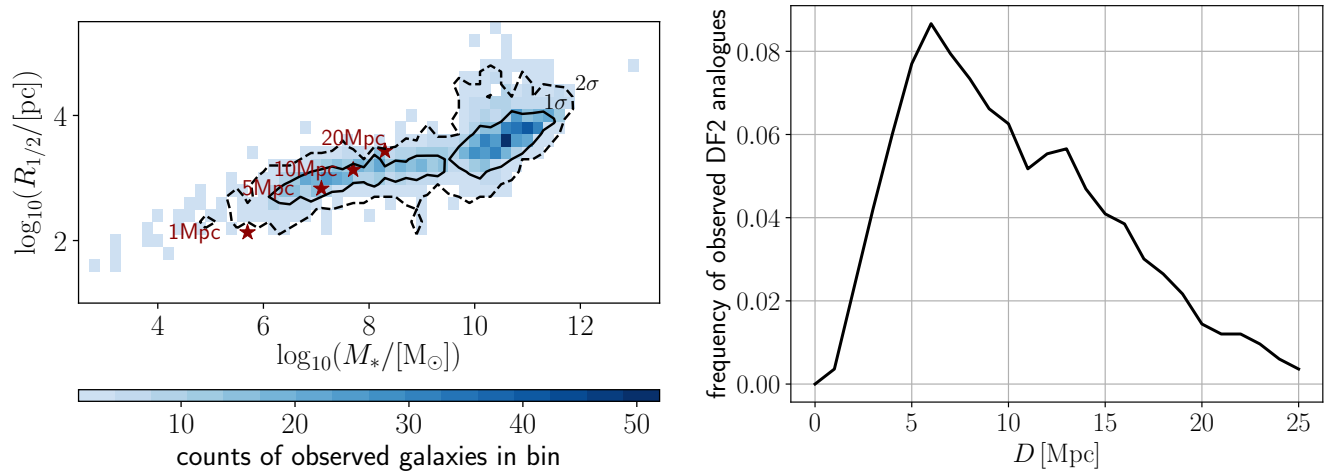


**Figure 12.** Left: Radius–mass diagram for observed early-type galaxies taken from [Dabringhausen & Fellhauer \(2016\)](#). The solid and dashed lines mark the  $1\sigma$  and  $2\sigma$  confidence levels, respectively. The half-light radii of the early-type galaxies are converted to 3D deprojected half-light radii by multiplying them by a factor of  $4/3$  (see Appendix B in [Wolf et al. 2010](#)). Red stars show the position of DF2 scaled for different distances. DF2 is consistent with observed dwarf galaxies with  $M_* < 10^9 M_\odot$  at the  $(11 \pm 3)\%$  confidence level if located at  $D = 20\text{Mpc}$ . Right: Distance-dependent probability density of observed DF2 analogues in the sample of [Dabringhausen & Fellhauer \(2016\)](#) with  $M_* < 10^9 M_\odot$  calculated by extracting all bin values along the locus of possible DF2 positions in the radius–mass diagram (highlighted by red stars in the left-hand panel).

#### 4.2.3 TDGs in MOND cosmology

As already stated in Section 4.1.1, dark-matter-lacking galaxies are rare in current self-consistent hydrodynamical cosmological simulations. [Haslbauer et al. \(2019\)](#) reported that only 0.17% of all galaxies with  $10^7 < M_*/M_\odot < 10^9$  are dark-matter-free tidal dwarf galaxies in the Illustris-1 simulation. This is consistent with the work of [Müller et al. \(2018\)](#) in which they showed that finding phase-space correlated systems like around the Centaurus A galaxy is  $\lesssim 0.5\%$  in Illustris-1. The combined probability of simulated disc of satellites comparable to those of the Milky Way, Andromeda M31, and Centaurus A galaxy is about  $5.1 \times 10^{-9}$  relative to the Millennium II and Illustris-1 simulations, when considering that 3D information on the position of satellites is only available in these three systems ([Pawlowski et al. 2014](#); [Müller et al. 2018](#)). However, [Ibata et al. \(2014\)](#) found significant evidence for such systems to be ubiquitous. Alone the existence of phase-space correlated satellite galaxies is thus in extremely significant disagreement with  $\Lambda\text{CDM}$  theory ([Kroupa et al. 2005](#)).

It is expected that the number of TDGs is higher in a MONDian compared to a  $\Lambda\text{CDM}$  Universe. Due to stronger self-gravitation in MONDian dynamics, TDGs can be formed more easily and be longer lasting since they are more resilient against tides from their host galaxies. Indeed, [Renaud et al. \(2016\)](#) showed that Milgromian models of galaxy–galaxy encounters produce more substructures within the tidal tails. In fact, [Okazaki & Taniguchi \(2000\)](#) concluded that a large fraction of observed dwarf ellipticals can be old TDGs in a cosmology where  $\approx 1 - 2$  TDGs form in each galaxy–galaxy encounter and subsequently survive for a Hubble time. This seems unlikely in a  $\Lambda\text{CDM}$  framework because TDGs formed in one interaction are likely to be destroyed in a subsequent interaction. This is due to the higher

merger rate of galaxies caused by dynamical friction between dark matter halos.

#### 4.2.4 Estimated tension with $\Lambda\text{CDM}$ in light of DF4

We have shown that the DF2 dwarf galaxy is unexpected in standard cosmology. Taking into account the dynamical  $M/L$  value ([Martin et al. 2018](#)), the stellar mass, half-light radius, GC population, peculiar velocity, and its angle relative to that of the LG, the probability of finding DF2-like galaxies in a  $\Lambda\text{CDM}$  cosmology is  $4.8 \times 10^{-7}$  for a distance of  $20.0\text{Mpc}$  (see Table 8 in Section 3.5). This rises to a maximum of  $1.0 \times 10^{-4}$  for a distance of  $11.5\text{Mpc}$  based on TNG100-1. Estimating that accurate mass, distance, and velocity dispersion measurements exist for 100 galaxies, there is a  $\lesssim 10^{-2}$  ( $2.6\sigma$  tension) chance of having detected a DF2-like object if at  $D = 11.5\text{Mpc}$  and  $\lesssim 4.8 \times 10^{-5}$  ( $4.1\sigma$  tension) if at  $D = 20.0\text{Mpc}$ . Note for completeness that adopting the [van Dokkum et al. \(2018b\)](#)  $M/L$  value instead, the chance of detecting a DF2 like object if at  $D = 11.0\text{Mpc}$  is  $2.4 \times 10^{-3}$  ( $3.0\sigma$  tension) and  $3.6 \times 10^{-6}$  ( $4.6\sigma$  tension) if at  $D = 20.0\text{Mpc}$ . At the lower distance, DF2 would be marginally consistent with the  $\Lambda\text{CDM}$  paradigm if it is the only galaxy of its kind.

However, preliminary results suggest that DF4 also lacks dark matter and has similar properties to DF2 but with a smaller radial velocity and half-light radius ([van Dokkum et al. 2019](#)). The probability of DF4-like subhaloes in cosmological simulations without the constraint on its GC population is  $\leq 1.4 \times 10^{-4}$  for a distance of  $20.0\text{Mpc}$ , which is comparable with our estimated occurrence rate of DF2 analogues (see Table 5 in Section 3.1). This is a conservative approach because the GCs appear to be unusually bright if located at  $D = 20\text{Mpc}$  (i.e. all seven identified GCs of DF4



have absolute magnitudes  $M_{V,606} \leq -8.6$  mag, van Dokkum et al. 2019).

Thus, it is very unlikely that we have observed two such dark-matter-lacking galaxies with similar properties. Assuming again measurements for 100 galaxies the observations of DF2 and DF4 cause a  $5.8\sigma$  tension with  $\Lambda$ CDM theory if both are located at  $D = 20.0$  Mpc. Adopting  $D = 11.5$  Mpc for DF2 and  $D = 20.0$  Mpc for DF4, the tension becomes  $4.8\sigma$ . These estimates hold true assuming the  $M/L$  value by Martin et al. (2018). The  $M/L$  value by van Dokkum et al. (2018b) would instead lead to a  $6.2\sigma$  tension with  $\Lambda$ CDM if both galaxies lie at  $D = 20.0$  Mpc, while the tension would be  $5.1\sigma$  if DF2 lies at  $11.0$  Mpc and DF4 at  $D = 20.0$  Mpc. The van Dokkum et al. (2018b)  $M/L$  value would thus virtually falsify  $\Lambda$ CDM cosmology. DF4 has a lower radial velocity than DF2, so there is less of an issue with making its GCs normally bright by putting it at a lower distance. However, DF4 would be then much more compact and thus more problematic for  $\Lambda$ CDM (Fig. 8). A more detailed analysis of DF4 is left to a future investigation once more observational data on this galaxy become available.

## 5 CONCLUSION

The inferred lack of dark matter in the UDG DF2 by van Dokkum et al. (2018b) follows from a low intrinsic velocity dispersion of  $\sigma_{\text{intr}} < 10.5$  km s $^{-1}$  with 90% confidence derived from the motion of 10 unusual bright GCs. However, their conclusion of the discovery of a dark-matter-deficient galaxy relies on a distance of  $D = 20$  Mpc from Earth. DF2 and also DF4 may be satellites of NGC 1052 and the whole system may be located at a much shorter distance of  $\approx 10$  Mpc, making their GC populations comparable to those of other galaxies (Haghi et al. 2019). In the here presented analysis, we showed that finding similar galaxies in standard cosmology is extremely rare regardless of its actual distance from Earth. We summarize our results as follows:

Constraints on the stellar half-mass, stellar mass, and total-to-stellar mass ratio consistent with the physical description of Martin et al. (2018) cause a decrease of the frequency of DF2-like subhaloes in  $\Lambda$ CDM simulations by about two orders of magnitude. These structural properties of simulated subhaloes mildly prefer a distance of  $D = 11.5^{+4.0}_{-1.5}$  Mpc for the TNG100-1 simulation in which the structural probabilities become maximal.

However, at  $D \leq 13$  Mpc, DF2 has a high peculiar velocity wrt. the CMB of  $v_{\text{pec}} \geq 676$  km s $^{-1}$ , which differs from that of the LG by  $v_{\text{rel}} \geq 1112$  km s $^{-1}$  with a large angle of  $\theta \approx 117^\circ$ . Taking into account only the peculiar velocity wrt. the CMB and motion relative to LG-like subhaloes yields a maximum probability at  $D = 20.0$  Mpc (the limit of the prior) with a  $1\sigma$  ( $2\sigma$ ) lower limit of  $16.5$  Mpc ( $12.0$  Mpc). In particular, these peculiar velocity criteria alone decrease the frequency of DF2-like subhaloes by two orders of magnitude at  $D \lesssim 13$  Mpc and by about one order of magnitude at  $D \gtrsim 16$  Mpc. This distance-dependence of the peculiar velocity probability is caused by the peculiar velocity of DF2 wrt. the CMB reference frame rather than by its motion relative to the LG. Interestingly, the peculiar velocity probability is the same for TNG100-1 and the much larger TNG300-1 simulation in which longer wave modes and therefore more

massive galaxy clusters are included. We demonstrated that the velocity field of TNG300-1 has converged by comparing it with that of the Millennium simulation, which has about a two times larger box length than TNG300-1 (Section 4.1.2). Since the reduction of the frequency based on the peculiar velocity of DF2-like subhaloes is the same for both the TNG100-1 and TNG300-1 simulations and the fact that TNG100-1 has a much better resolution than TNG300-1, our main results rely on the former simulation run.

Such a high velocity, which arises if DF2 is at  $D \lesssim 13$  Mpc, is not impossible in  $\Lambda$ CDM cosmology, but reduces the detection probability of simulated DF2 analogues for lower distances significantly. It is interesting to point out that high peculiar velocities can be occasionally observed in the real Universe and are likely in Milgromian gravitation, but not in  $\Lambda$ CDM cosmology (Section 4.1.2 in this work and Fig. 14 in Candlish 2016). Thus, the detection probability of DF2 analogues located at  $D \leq 13$  Mpc is higher in a MOND cosmology, because the velocity field would be shifted to higher values compared to that of the  $\Lambda$ CDM model. However, so far and for a variety of reasons not related to technical issues, there are no self-consistent hydrodynamical MOND cosmological simulations available which would allow a detailed comparison of the structural properties, masses, and kinematics of MONDian dwarf galaxies with observations.

Considering the structural properties and peculiar velocity of subhaloes, cosmological  $\Lambda$ CDM simulations suggest that DF2 analogues occur with a probability of  $1.2 \times 10^{-3}$  for a distance of  $20.0$  Mpc. The  $1\sigma$  ( $2\sigma$ ) lower distance limit is  $16.0$  Mpc ( $11.5$  Mpc) based on TNG100-1 (Section 3.1).

The observed DF2 galaxy and presumably also DF4 have an extremely unusual GC population if located at  $D = 20$  Mpc. Bringing DF2 to a much smaller distance of about  $D = 10 - 13$  Mpc makes the luminosities and structural properties of its GC population comparable with that in other observed galaxies (Sections 3.2 and 3.3) as also concluded by Trujillo et al. (2019). Since GCs are in the high-acceleration regime of MOND, the GC population of DF2 is independent of the cosmological model and would therefore challenge any cosmological model if at  $D = 20$  Mpc.

Combining the results from the cosmological  $\Lambda$ CDM simulation with the luminosity of the GC population, DF2 is statistically expected at a distance of  $D = 11.5 \pm 1.5$  Mpc with a maximal probability of  $1.0 \times 10^{-4}$  based on TNG100-1 (Section 3.5). Restricting this analysis only for DF2 analogues embedded in host halos with  $M_{200} \leq 10^{13} M_\odot$  reduces the probability again by about one order of magnitude and yields a most likely distance of  $D = 13.0 \pm 1.5$  Mpc (Appendix B). Thus, our results are consistent with Trujillo et al. (2019). This is in disagreement with the results of van Dokkum et al. (2018d) who argued that DF2 cannot be located at  $D \leq 13$  Mpc. However, Trujillo et al. (2019) derived a distance of  $13.0 \pm 0.4$  Mpc based on redshift-independent indicators. If DF2 is located at  $20.0$  Mpc as proposed by van Dokkum et al. (2018b), its combined probability of occurrence in standard cosmology is  $\leq 4.8 \times 10^{-7}$  (Section 4.2.4).

The chance of detecting DF4-like subhaloes in cosmological simulations without the constrain on its GC population is  $\leq 1.4 \times 10^{-4}$  for a distance of  $20.0$  Mpc (Section 3.1). We have not studied the GC population and frequency

of DF4-like objects over distance, because precise measurements of its GC population are not publicly available yet.

Taking into account that precise measurements exist for 100 galaxies, DF2 is in tension with standard cosmology at  $2.6\sigma$  ( $4.1\sigma$ ) if located at 11.5 Mpc (20.0 Mpc). Adopting the former distance for DF2 and ignoring the GC population of DF4, both dark matter lacking galaxies would cause a  $4.8\sigma$  tension. Placing both galaxies at  $D = 20.0$  Mpc results in a rejection of the  $\Lambda$ CDM cosmology by  $5.8\sigma$ . If the recently observed DF4 dwarf galaxy (van Dokkum et al. 2019) has a similar GC population to DF2, the tension with  $\Lambda$ CDM becomes even more significant (Section 4.2.4). Therefore, the observed properties of dwarf galaxies may point to the need for new physics.

## ACKNOWLEDGEMENTS

We thank the anonymous referee for her/his suggested improvements. IB is supported by an Alexander von Humboldt postdoctoral research fellowship. KG was supported by the German-Russian Interdisciplinary Science Center funded by the German Federal Foreign Office via the German Academic Exchange Service. We thank Graeme Candlish for sharing his data on the velocity field in MOND cosmology and Hosein Haghi for useful discussions about the properties of NGC 1052-DF2.

## REFERENCES

- Angus G. W., McGaugh S. S., 2008, *MNRAS*, **383**, 417
- Banik I., Zhao H., 2017, *MNRAS*, **467**, 2180
- Barnes J. E., Hernquist L., 1992, *Nature*, **360**, 715
- Bekenstein J., Milgrom M., 1984, *ApJ*, **286**, 7
- Bournaud F., Duc P.-A., 2006, *A&A*, **456**, 481
- Bournaud F., Bois M., Emsellem E., Duc P.-A., 2008a, *Astron. Nachr.*, **329**, 1025
- Bournaud F., Duc P.-A., Emsellem E., 2008b, *MNRAS*, **389**, L8
- Candlish G. N., 2016, *MNRAS*, **460**, 2571
- Chowdhury A., 2019, *MNRAS*, **482**, L99
- Dabringhausen J., Fellhauer M., 2016, *MNRAS*, **460**, 4492
- Dabringhausen J., Kroupa P., 2013, *MNRAS*, **429**, 1858
- Danieli S., van Dokkum P., Conroy C., Abraham R., Romanowsky A. J., 2019, *ApJ*, **874**, L12
- Davies R. L., Illingworth G. D., 1986, *ApJ*, **302**, 234
- Davis M., Efstathiou G., Frenk C. S., White S. D. M., 1985, *ApJ*, **292**, 371
- De Lucia G., Springel V., White S. D. M., Croton D., Kauffmann G., 2006, *MNRAS*, **366**, 499
- Denicoló G., Terlevich R., Terlevich E., Forbes D. A., Terlevich A., Carrasco L., 2005, *MNRAS*, **356**, 1440
- Dolag K., Borgani S., Murante G., Springel V., 2009, *MNRAS*, **399**, 497
- Emsellem E., et al., 2019, *A&A*, **625**, A76
- Famaey B., McGaugh S., Milgrom M., 2018, *MNRAS*, **480**, 473
- Fensch J., et al., 2019, *A&A*, **625**, A77
- Forbes D. A., Sinpetru L., Savorgnan G., Romanowsky A. J., Usher C., Brodie J., 2017, *MNRAS*, **464**, 4611
- Fouquet S., Hammer F., Yang Y., Puech M., Flores H., 2012, *MNRAS*, **427**, 1769
- Genel S., et al., 2014, *MNRAS*, **445**, 175
- Graus A. S., Bullock J. S., Boylan-Kolchin M., Nierenberg A. M., 2018, *MNRAS*, **480**, 1322
- Haghi H., et al., 2019, *MNRAS*, **487**, 2441
- Harris W. E., 1996, *AJ*, **112**, 1487
- Haslbauer M., Dabringhausen J., Kroupa P., Javanmardi B., Banik I., 2019, *A&A*, **626**, A47
- Hinshaw G., et al., 2013, *ApJS*, **208**, 19
- Ibata N. G., Ibata R. A., Famaey B., Lewis G. F., 2014, *Nature*, **511**, 563
- Jeřábková T., Hasani Zonoozi A., Kroupa P., Beccari G., Yan Z., Vazdekis A., Zhang Z.-Y., 2018, *A&A*, **620**, A39
- Kogut A., et al., 1993, *ApJ*, **419**, 1
- Kraljic D., Sarkar S., 2015, *J. Cosmology Astropart. Phys.*, **2015**, 050
- Kroupa P., 1995, *ApJ*, **453**, 350
- Kroupa P., 2012, *Publ. Astron. Soc. Australia*, **29**, 395
- Kroupa P., Weidner C., 2003, *ApJ*, **598**, 1076
- Kroupa P., Theis C., Boily C. M., 2005, *A&A*, **431**, 517
- Kroupa P., et al., 2010, *A&A*, **523**, A32
- Kroupa P., et al., 2018, *Nature*, **561**, E4
- Lynden-Bell D., Faber S. M., Burstein D., Davies R. L., Dressler A., Terlevich R. J., Wegner G., 1988, *ApJ*, **326**, 19
- Mann H. B., Whitney D. R., 1947, *Ann. Math. Stat.*, **18**, 50
- Marinacci F., et al., 2018, *MNRAS*, **480**, 5113
- Martin N. F., Collins M. L. M., Longeard N., Tollerud E., 2018, *ApJ*, **859**, L5
- McAlpine S., et al., 2016, *Astron. and Comput.*, **15**, 72
- Milgrom M., 1983, *ApJ*, **270**, 365
- Milgrom M., 2010, *MNRAS*, **403**, 886
- Molnar S. M., Broadhurst T., 2015, *ApJ*, **800**, 37
- Müller O., Pawłowski M. S., Jerjen H., Lelli F., 2018, *Science*, **359**, 534
- Müller O., Famaey B., Zhao H., 2019, *A&A*, **623**, A36
- Naiman J. P., et al., 2018, *MNRAS*, **477**, 1206
- Nelson D., et al., 2015, *Astron. Comput.*, **13**, 12
- Nelson D., et al., 2018, *MNRAS*, **475**, 624
- Nelson D., et al., 2019, *Comput. Astrophys. Cosmol.*, **6**, 2
- Nusser A., 2019, *MNRAS*, **484**, 510
- Okazaki T., Taniguchi Y., 2000, *ApJ*, **543**, 149
- Pawłowski M. S., McGaugh S. S., 2014, *MNRAS*, **440**, 908
- Pawłowski M. S., Kroupa P., Jerjen H., 2013, *MNRAS*, **435**, 1928
- Pawłowski M. S., et al., 2014, *MNRAS*, **442**, 2362
- Peebles P. J. E., submitted, preprint, *Arxiv* (arXiv:1705.10683v1)
- Pillepich A., et al., 2018a, *MNRAS*, **473**, 4077
- Pillepich A., et al., 2018b, *MNRAS*, **475**, 648
- Planck Collaboration et al., 2014, *A&A*, **571**, A16
- Planck Collaboration et al., 2016, *A&A*, **594**, A13
- Ploeckinger S., Sharma K., Schaye J., Crain R. A., Schaller M., Barber C., 2018, *MNRAS*, **474**, 580
- Rejkuba M., 2012, *Ap&SS*, **341**, 195
- Renaud F., Famaey B., Kroupa P., 2016, *MNRAS*, **463**, 3637
- Sardone A., Pisano D. J., Burke-Spolaor S., Mascoop J. L., Pol N., 2019, *ApJ*, **871**, L31
- Schaye J., et al., 2015, *MNRAS*, **446**, 521
- Spolaor M., Forbes D. A., Hau G. K. T., Proctor R. N., Brough S., 2008, *MNRAS*, **385**, 667
- Springel V., 2005, *MNRAS*, **364**, 1105
- Springel V., 2010, *MNRAS*, **401**, 791
- Springel V., White S. D. M., Tormen G., Kauffmann G., 2001, *MNRAS*, **328**, 726
- Springel V., et al., 2005, *Nature*, **435**, 629
- Springel V., et al., 2018, *MNRAS*, **475**, 676
- Trujillo I., et al., 2019, *MNRAS*, **486**, 1192
- Tully R. B., 2015, *AJ*, **149**, 54
- Vogelsberger M., et al., 2014a, *MNRAS*, **444**, 1518
- Vogelsberger M., et al., 2014b, *Nature*, **509**, 177
- Watts A. B., Meurer G. R., Lagos C. D. P., Bruzzone S. M., Kroupa P., Jerabkova T., 2018, *MNRAS*, **477**, 5554
- Wetzstein M., Naab T., Burkert A., 2007, *MNRAS*, **375**, 805

- Wolf J., Martinez G. D., Bullock J. S., Kaplinghat M., Geha M., Muñoz R. R., Simon J. D., Avedo F. F., 2010, *MNRAS*, **406**, 1220
- Yan Z., Jerabkova T., Kroupa P., 2017, *A&A*, **607**, A126
- Yang Y., Hammer F., Fouquet S., Flores H., Puech M., Pawlowski M. S., Kroupa P., 2014, *MNRAS*, **442**, 2419
- Yu H., Ratra B., Wang F.-Y., submitted, preprint, *Arxiv* (arXiv:1809.05938v1)
- Zonoozi A., Haghi H., Kroupa P., in prep.
- van Dokkum P., et al., 2018a, *Res. Notes of the Am. Astron. Soc.*, **2**, 54
- van Dokkum P., et al., 2018b, *Nature*, **555**, 629
- van Dokkum P., et al., 2018c, *ApJ*, **856**, L30
- van Dokkum P., Danieli S., Cohen Y., Romanowsky A. J., Conroy C., 2018d, *ApJ*, **864**, L18
- van Dokkum P., Danieli S., Abraham R., Conroy C., Romanowsky A. J., 2019, *ApJ*, **874**, L5

## APPENDIX A: SCALING OBSERVABLES TO DIFFERENT DISTANCES

In order to scale the properties to different distances,  $D$ , we apply in Sections 2.3, 3, and 4 the following scaling relations for the stellar mass,  $M_*$ , stellar half-mass radius,  $R_{1/2}$ , total-to-stellar ratio,  $M_{\text{total}}/M_*$ , and luminosity,  $L$ :

$$M_* \propto D^2, \quad (\text{A1})$$

$$R_{1/2} \propto D, \quad (\text{A2})$$

$$M_{\text{total}}/M_* \propto D^{-1}, \quad (\text{A3})$$

$$L \propto D^2. \quad (\text{A4})$$

## APPENDIX B: COMBINED PROBABILITIES

DF2 and the massive elliptical galaxy NGC 1052 have a statistically expected 3D separation of about 100 kpc if located at 20 Mpc (van Dokkum et al. 2018b). Thus, within the  $\Lambda$ CDM framework DF2 can be embedded in the main halo of NGC 1052, which has a mass of  $M_{200} \approx 10^{13} M_{\odot}$  estimated from the stellar mass of NGC 1052 ( $M_* \approx 10^{11} M_{\odot}$ ). Therefore, only DF2-like subhaloes embedded in host halos with  $M_{200} \leq 10^{13} M_{\odot}$  are included in Fig. B1. As in Section 3.5 the probability is maximal in the TNG100-1 simulation and DF2 is most likely at  $D = 13.0 \pm 1.5$  Mpc with a probability of  $5.2 \times 10^{-6}$  ( $4.6\sigma$ ). For the Illustris-1, TNG100-1, and TNG300-1 the probability is reduced by a factor of  $\approx 10$ . The results of the EAGLE-1 simulation are not much affected, because here the probability is already quite low. No DF2 analogues can be found for  $D < 17$  Mpc and  $D < 18$  Mpc in the EAGLE-1 and Illustris-1 simulations, respectively.

This paper has been typeset from a  $\text{\TeX}/\text{\LaTeX}$  file prepared by the author.

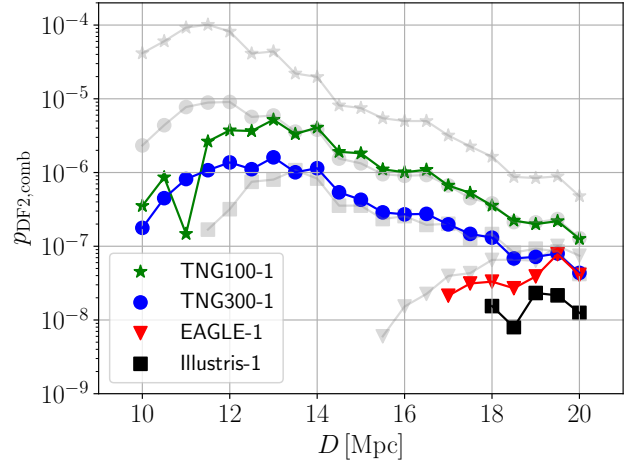


**Figure B1.** Same as Fig. 7 (grey data points) but only for DF2-like subhaloes embedded in host halos with  $M_{200} \leq 10^{13} M_{\odot}$ . There are no DF2-like subhaloes in the EAGLE-2 and EAGLE-3 simulations.